Int J Earth Sci (Geol Rundsch) (2016) 105:2075–2096
DOI 10.1007/s00531-015-1255-2

ORIGINAL PAPER

Ductile nappe stacking and refolding in the Cycladic Blueschist Unit: insights from Sifnos Island (south Aegean Sea)

Eirini Aravadinou[1] · Paraskevas Xypolias[1] · Vasileios Chatzaras[2,3] · Ioannis Iliopoulos[1] · Nikolaos Gerogiannis[1]

Received: 16 May 2015 / Accepted: 29 September 2015 / Published online: 16 October 2015

Abstract New geological and structural mapping combined with kinematic and amphibole chemistry analyses is used to investigate the deformation history of the Cycladic Blueschist Unit (CBU) on Sifnos Island (Cyclades, Aegean Sea). We concentrate on north Sifnos, an area characterized by exceptionally well-preserved eclogites and blueschists. Our data show that the early, main phase (D_2) of ductile deformation in the CBU occurred synchronous with the transition from prograde to close-to-peak retrograde conditions. This deformation phase took place at middle Eocene and is related to ESE-directed thrusting that emplaced the metavolcano-sedimentary subunit over the Marble subunit. The subsequent exhumation-related (D_3) deformation is characterized by gently NE-plunging folds and NE-directed contractional shear zones that formed parallel to the axial planes of folds. NE-directed shearing occurred under blueschist and transitional blueschist-/greenschist-facies conditions during late Eocene–Oligocene and caused the restacking of the early nappe pile. We suggest that a mechanism of ductile extrusion of the CBU in a tectonic setting of net compression could explain better the recorded exhumation-related deformation than a mechanism of syn- and post-orogenic extension. Our new kinematic results in combination with previous works in the Cyclades area reveal a regional scale change in tectonic transport direction from (W)NW–(E)SE at Late Cretaceous–middle Eocene to (E)NE–(W)SW at late Eocene–Oligocene times. The observed change in transport direction may be governed by the relative motion of Africa with respect to Europe during Alpine orogeny.

Keywords Blueschist · Ductile thrust · Ductile deformation · Hellenides · High-pressure metamorphism

Introduction

The area of north Sifnos is well known in geological literature for its extensive exposures of exceptionally well-preserved eclogites and blueschists of the Cycladic Blueschist Unit (Fig. 1a, b) (Okrusch and Bröcker 1990; Schliestedt and Matthews 1987; Avigad 1993). The high-pressure (HP) rocks were formed during early–middle Eocene in the course of the Alpine orogenesis in eastern Mediterranean region (e.g., Maruyama et al. 1996). Works on the structural evolution of the area are limited (Avigad 1993; Trotet et al. 2001a), lagging significantly behind numerous petrological and isotopic studies (e.g., Altherr et al. 1979; Matthews and Schliestedt 1984; Evans 1986; Ganor et al. 1989; Wijbrans et al. 1990; Lister and Raouzaios 1996; Mocek 2001; Trotet et al. 2001b; Schmädicke and Will 2003; Groppo et al. 2009; Bröcker et al. 2013; Dragovic et al. 2015). Undoubtedly, the structural analysis of eclogite- and blueschist-facies rocks is critically important for unraveling the deformation history of HP belts from the early, deep burial stages to subsequent exhumation and thus to retrieve valuable information for the tectonic processes occurring

Electronic supplementary material The online version of this article (doi:10.1007/s00531-015-1255-2) contains supplementary material, which is available to authorized users.

✉ Paraskevas Xypolias
p.xypolias@upatras.gr

[1] Department of Geology, University of Patras, 26500 Patras, Greece

[2] Department of Geoscience, University of Wisconsin-Madison, Madison, WI 53706, USA

[3] Department of Earth Sciences, Utrecht University, PO Box 80.021, 3508 TA Utrecht, The Netherlands

during subduction. Commonly, it is hard, if not impossible, to detect structural data for the full subduction–exhumation cycle. The early deformation history is masked by the polyphase structural overprint, which typically characterizes metamorphic belts, and the textural and mineralogical transformations during rock exhumation. In the CBU, the kinematics associated with the prograde deformation stage is poorly known. With few exceptions (north Sifnos, Syros, and south Evia; Fig. 1b), the exhumation-related deformation and the associated greenschist-facies retrogression have almost obliterated the early deformation structures/fabrics (Jolivet et al. 2003). Commonly, the entire tectonometamorphic evolution of the CBU is attributed to a single NNE-dipping subduction zone, which controlled the tectonic evolution of the Hellenides from the Mesozoic until present (Bonneau 1984; Jolivet and Brun 2010; Ring et al. 2010; Papanikolaou 2013). However, structural data from well-preserved blueschists in Syros (Ridley 1982, 1986) and south Evia (Xypolias et al. 2012) indicate (E)SE-directed thrusting during Eocene HP metamorphism, putting in doubt the previous scenario. Therefore, north Sifnos provides a unique opportunity to bring new data for the kinematics of the CBU at the deeper parts of the subduction zone.

Due to the poor preservation of early structures, most structural studies in Cyclades have focused on the deformation associated with the exhumation of the CBU. However, despite numerous studies over the last decades, there is still no consensus concerning the exhumation mechanism of the Cycladic HP rocks, and the time of initiation of back-arc extension in the south Aegean Sea. The proposed mechanisms can be grouped into two main contrasting modes: exhumation due to crustal-scale extension and exhumation under an overall crustal shortening. In the first mode, the CBU was exhumed in the footwall of a series of shallow, NE-dipping extensional detachments. The extensional detachments formed deep in the accretionary complex during Eocene (syn-orogenic stage) and then accommodated back-arc-related extension in Oligocene–late Miocene times (post-orogenic stage) (Avigad et al. 1997; Forster and Lister 2009; Jolivet and Brun 2010). According to this model, well-preserved eclogites and blueschists, such as those in north Sifnos, occur in close proximity to the syn-orogenic detachments (Trotet et al. 2001a). In the second mode, late Eocene–early Miocene exhumation (ductile stage) of the CBU occurred within an extrusion wedge (Xypolias et al. 2003, 2012; Ring et al. 2007). This wedge is bounded by a subduction-related thrust fault at the base and an upper crustal-scale normal-sense fault operating under an overall shortening regime similar to that occurring in Himalayas (e.g., Hodges et al. 1992; Godin et al. 2006; Montomoli et al. 2013). The subsequent exhumation (brittle stage) was controlled by Miocene back-arc extension. Therefore, these contrasting interpretations clearly indicate the need for more detailed studies of the exhumation-related structures, to discriminate among the different modes of exhumation.

In this work, we present a new detailed geological and structural map of north Sifnos, an area previously mapped in reconnaissance by Davis (1966) and Matthews and Schliestedt (1984) (Fig. 1c). The mapping results, in combination with new mesoscale structural, microstructural and amphibole chemistry analyses, are used to provide further insights into the tectonometamorphic evolution of the CBU. We focus on the kinematics at the deep parts of subduction channel, as well as on the deformation pattern associated with the ductile-stage exhumation.

Geological framework

The orogenic belt of the Hellenides is developed during the Alpine orogenesis, following the closure of a series of Neo-Tethyan oceanic strands and the consequent multiphase continent–continent collision between Eurasia and Gondwana-derived fragments (Robertson and Dixon 1984; Doutsos et al. 1993; Xypolias and Doutsos 2000; Zulauf et al. 2008; Papanikolaou 2009; Kilias et al. 2010; van Hinsbergen and Schmid 2012). The Cycladic Massif and its structurally overlying Pelagonian Zone belong to the Internal Hellenides. They form a NW-striking belt bordered by the Pindos and Vardar ophiolitic sutures (Fig. 1a) (Jacobshagen 1986; Robertson 2002; Dilek et al. 2007). The Pelagonian Zone consists of pre-Alpine basement rocks and Mesozoic marbles (Mountrakis 1986).

The Cycladic Massif comprises a pile of nappes/units that were mainly stacked at Eocene and Oligocene times (Avigad et al. 1997; Xypolias et al. 2003, 2010; Ring et al. 2007). The CBU occupies an intermediate structural position within the Cycladic nappe pile and possible represents a metamorphosed late Paleozoic–Mesozoic succession which was developed in a passive rift or a back-arc setting (Dürr 1986; Mocek 2001; Keiter et al. 2011; Chatzaras et al. 2013). The CBU mainly consists of marbles, metapelites and metavolcanic rocks. Locally (e.g., Evia, Andros, Syros), it passes upwards to a metaophiolite bearing and often chaotic metavolcano-sedimentary (MVS) complex (Keiter et al. 2011; Xypolias et al. 2012). The metamorphic history of the CBU includes an Eocene (ca. 50–40 Ma) eclogite- to blueschist-facies metamorphic event, overprinted by an early Miocene (ca. 23–21 Ma) greenschist-facies metamorphism (Bröcker et al. 2004; Katzir et al. 2000; Maluski et al. 1981; Tomaschek et al. 2003). The early Miocene metamorphism increases locally from greenschist facies up to partial melting, producing migmatite domes (Kruckenberg et al. 2011 and references

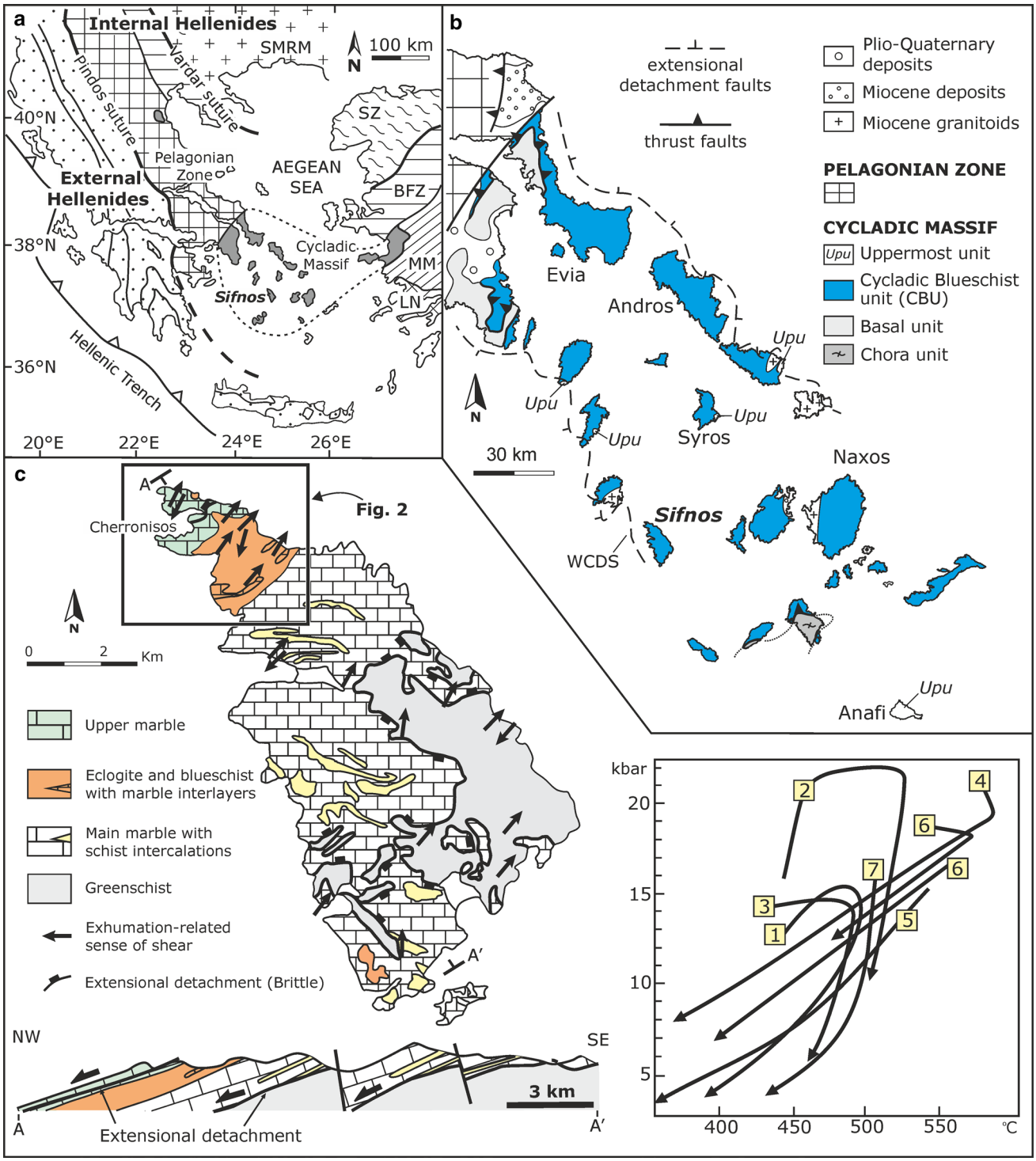

Fig. 1 **a** Simplified geological map of the Aegean region showing the major tectonic units and the position of the Cycladic Massif in the Internal Hellenides (*BFZ* Bornova Flysch Zone, *LN* Lycian Nappes, *MM* Menderes Massif, *SZ* Sakarya Zone, *SMRM* Serbomacedonian and Rhodope Massifs). **b** Simplified geological map of the central–western part of the Cycladic Massif (*WCDS* West Cycladic Detachment System). **c** Geological map of Sifnos Island (after Davis 1966; Matthews and Schliestedt 1984; Avigad 1993) showing the major lithological subunits and the position of low-angle extensional detachments; exhumation-related sense of shear after Trotet et al. (2001a). *Box* indicates the location of the map in Fig. 2. The geological section *A*–*A*′ shows the structure of the CBU in Sifnos Island; after Avigad (1993) and Trotet et al. (2001a). *Inset* shows different proposed P–T paths for CBU in Sifnos [*1* Matthews and Schliestedt (1984) and Schliestedt and Matthews (1987); *2* Groppo et al. (2009); *3* Schliestedt (1990); *4* Trotet et al. (2001b); *5* Avigad (1993); *6* Schmädicke and Will (2003); *7* Avigad et al. (1992)]

therein). Commonly, the greenschist retrogression becomes increasingly dominant toward the lower structural levels of the CBU (Bröcker et al. 2004). Greenschist retrogression is also broadly synchronous with the localization of ductile deformation at the base of the unit (e.g., Xypolias et al. 2003, 2010). The CBU is tectonically emplaced over either a pre-Alpine crystalline basement (known as Chora unit; Bonneau 1984) or the Basal unit (Xypolias et al. 2010). The Basal unit consists of Mesozoic marbles capped by an early Cenozoic metaflysch (Avigad et al. 1997). Both Chora and Basal units have been affected by Alpine HP metamorphism (Franz et al. 1993; Shaked et al. 2000). The CBU, in turn, is overlain by the Uppermost unit consisting of Late Cretaceous granitoids, Paleocene amphibolites and greenschists, and marbles showing no evidence of Alpine HP metamorphism (e.g., Reinecke et al. 1982).

Geology of Sifnos

The rocks on Sifnos Island belong to the CBU and form a ca. 2500-m-thick metamorphic pile, which is commonly subdivided, from structurally highest to lowest, into the following four subunits (Fig. 1c) (Davis 1966; Matthews and Schliestedt 1984; Okrusch and Bröcker 1990; Avigad 1993). (a) The *Upper Marble subunit* is composed of calcite and locally dolomite marbles with minor intercalations of quartzite. Glaucophanites, blueschists and mica schists are exposed on the top of the subunit. (b) The *Eclogite–Blueschist subunit* represents a MVS subunit consisting of alternations of basic metavolcanic (glaucophanites and eclogites) and felsic metavolcanic (jadeite–quartz gneisses) rocks, and interlayers of metasediments (mica schists, calcite schist, quartzites and marbles). (c) The *Main Marble subunit* is chiefly made up of calcite marbles. Dolomite marble interlayers occur mainly at the lower parts of the subunit, while calcite schists and greenschists with relics of eclogites and glaucophanites are preserved as intercalations up to 50 m thick. (d) The *Greenschist subunit* consists of a MVS rock assemblage equivalent to those of the Eclogite–Blueschist subunit including metasediments, metabasites and metaacidites of middle Triassic protolith age (Bröcker and Pidgeon 2007). This rock assemblage has been widely transformed into greenschist-facies rocks. Evidence of an earlier HP metamorphism is provided by relic eclogite and glaucophanite lenses.

Several pressure (P)–temperature (T) paths have been proposed for the metamorphic evolution of the CBU in Sifnos, which are schematically summarized in Fig. 1c. Generally, peak P–T conditions have been estimated at 450–550 °C and 15–20 kbar (Groppo et al. 2009 and references therein), while the thermal peak mineral assemblage recorded in Eclogite–Blueschist subunit includes garnet, omphacite, sodic amphibole and paragonite (Schmädicke and Will 2003). The greenschist-facies assemblages equilibrated at 350–450 °C and 6–9 kbar revealing cooling during decompression (e.g., Avigad et al. 1992; Schmädicke and Will 2003). Schmädicke and Will (2003) emphasized that Eclogite–Blueschist and Greenschist subunits show no differences in their retrograde P–T trends revealing a progressive equilibration from blueschist- to greenschist-facies conditions rather than retrograde overprint due to a distinct medium-pressure Barrovian-type thermal event as suggested by others (Wijbrans et al. 1990; Forster and Lister 2005). K–Ar, $^{40}Ar/^{39}Ar$ and Rb–Sr phengitic mica ages for transitional blueschist–greenschist and greenschist-facies rocks vary from 41 to 19 Ma (Altherr et al. 1979; Wijbrans et al. 1990; Forster and Lister 2005; Ring et al. 2011; Bröcker et al. 2013). This large age variation is interpreted to indicate a continuous resetting of the isotopic system, or mica recrystallization during exhumation and progressive equilibration to greenschist-facies conditions (Bröcker et al. 2013). Isotopic dating of fresh blueschist samples yielded K–Ar and $^{40}Ar/^{39}Ar$ phengite ages of ca. 42–47 Ma (Altherr et al. 1979; Wijbrans et al. 1990). Sm/Nd ages of ca. 46 Ma for garnet, grown at 490–550 °C and 22 kbar, possibly date the peak of HP metamorphism (Dragovic et al. 2012, 2015).

In terms of deformation history, previous works have highlighted at least four deformation phases, which affected heterogeneously the Eclogite–Blueschist and the Greenschist subunits. Evidence for the first deformation phase is sparse and expressed in the form of an internal foliation in pre-tectonic garnet porphyroblasts with respect to subsequent deformation (Lister and Raouzaios 1996). The internal foliation is defined by omphacite, glaucophane, epidote and mica and possible developed at an early stage of the eclogite-facies metamorphism (Lister and Raouzaios 1996; Groppo et al. 2009). The second deformation phase is associated with the formation of an Eclogite–Blueschist S_2 foliation, which is formed at peak metamorphic conditions (Lister and Raouzaios 1996; Groppo et al. 2009) or during the first retrogression stage (Trotet et al. 2001a). According to Trotet et al. (2001a), S_2 is accompanied by a prominent NE–SW-trending mineral lineation and top-to-the-NE sense of shear. Lister and Raouzaios (1996) suggest that the S_2 foliation was pervasively developed over the island, but it was strongly disrupted by subsequent deformation events. Generally, there is consensus that the subsequent phases of ductile deformation (at least two phases) were associated with top-to-(N)NE shear sense and caused the exhumation of rocks from Eclogite–Blueschist to greenschist-facies conditions (Avigad 1993; Lister and Raouzaios 1996; Trotet et al. 2001a). The deformation during these phases was mainly localized in the Greenschist subunit and was produced NE–SW-trending lineation(s) accompanied by penetrative foliation(s) (Trotet et al. 2001a) or an

axial planar foliation of overturned, NW-trending meso- to map-scale folds (Avigad 1993). On the basis of this deformation history, it is suggested that syn- and post-orogenic crustal-scale extension was accommodated by shallow, NE-dipping detachment faults. These extensional detachments were active from Eocene (eclogite facies) to Miocene (greenschist and subgreenschist facies), under a continuum of top-to-the-NE ductile shear, which led to the progressive exhumation of HP rocks (Fig. 1c; A–A′) (Trotet et al. 2001a; Jolivet et al. 2013). Avigad (1993) proposed that the contact between the Main Marble subunit and the underlying Greenschist subunit is a brittle, NE-dipping extensional detachment fault resulting in the juxtaposition of the Eclogite–Blueschist and Greenschist subunits after the greenschist-facies metamorphism. Recently, Ring et al. (2011) showed that this extensional detachment is associated with top-to-the-SSW shearing and limited displacement of the order of few kilometers since represents the south termination of West Cycladic Detachment System (Fig. 1b; Grasemann et al. 2012), which operated at early–middle Miocene. In turn, Lister and Raouzaios (1996) suggested, based on metamorphic criteria, that exhumation-related deformation is associated with the north-directed thrusting of the Eclogite–Blueschist subunit over the underlying subunits. All these interpretations are critically examined on the basis of new data presented here. Our work adds upon the previously described deformation history and provides a detailed analysis of the deformation style of each of the superimposed phases. Emphasis is given on the nature of tectonic contacts, as well as on the composition of amphiboles that define the major deformation fabrics.

Mapping results and structural evolution

In order to understand the structural architecture of the CBU in north Sifnos, we carried out detailed geological–structural mapping. The new map is illustrated in Fig. 2. In terms of lithology, we have distinguished two main subunits: the *Marble* subunit, which includes the above-defined Upper Marble and Main Marble subunits, and the MVS subunit (Figs. 1c, 2). It is noted that the Upper Marble and the Main Marble subunits are unified into a single subunit, mainly based on two criteria: (a) there are no lithological differences between these marble exposures, and (b) a package of volcanic rocks (the main protolith of MVS) sandwiched between two pure carbonate layers, which show no evidence for intrusions, could not be a primary association but possibly the result of tectonic repetition. Note that the volcanic protoliths of the MVS were formed in an island-arc setting that evolved to a back-arc environment (Mocek 2001). Also, the latter criterion is further supported by structural data presented below (i.e., all contacts between the marbles and the MVS subunit are mylonitic).

The Marble subunit is composed of gray- to white-colored calcite marbles with dolomite and quartzite intercalations. It also includes mappable layers of dolomite marbles with minor intercalations of calcite marbles (Fig. 2). The dolomitic component increases toward the lower (tectono-) stratigraphic levels of the Marble subunit. Two rock complexes, which are dominated by glaucophanites and felsic orthogneisses, respectively, were mapped into the MVS subunit. The glaucophanite complex consists of garnetiferous glaucophanites, garnet–glaucophane schist and sporadic eclogite bands (continuous or lensoid in shape) with local interlayers of mica schist and felsic orthogneiss. The complex of felsic orthogneiss is generally lithologically homogeneous and is dominated by garnetiferous fine-grained quartz–albite gneiss with minor concordant interlayers of glaucophanite, mainly close to the contact with the glaucophanite complex. Typically, the contacts between the two complexes of the MVS subunit are gradational and blurred. This feature probably reflects original interfingering between the basic and felsic volcanic protoliths.

Our field-based work on north Sifnos enabled us to unravel a polyphase deformation history characterized by three main phases of ductile deformation (D_1–D_3). All ductile structures/fabrics have been overprinted by (N)NE- and NW-striking brittle normal faults (Fig. 2). Different generations of ductile structures/fabrics were distinguished on the basis of overprinting criteria observed at map to outcrop scale, differences in structural style and orientation, as well as relationships between mineral growth and deformation fabrics. The recognized deformation phases are described below in a chronological order from older to younger. The structural data, upon which is based the distinction of phases, are synthesized in the geological–structural map (Fig. 2) and the corresponding detailed cross sections (Fig. 3) depicting the internal structural architecture of the CBU. Orientation data are summarized in equal-area plots (Fig. 4).

D_1–D_2 deformation phases: early nappe stacking

Early ductile structures are mainly preserved in competent lithologies (i.e., eclogite, glaucophanite) and represented by the S_1 and S_2 foliations. The S_1 foliation can be locally recognized where it wraps around the hinges of isoclinal, intrafolial F_2 folds having been transposed into a composite $S_{1/2}$ foliation, which is parallel to the F_2 axial planes (Fig. 5a, b). $S_{1/2}$ foliation is mainly defined by the alignment of glaucophane, omphacite and white mica. At the microscopic scale, evidence for the early S_1 fabric is

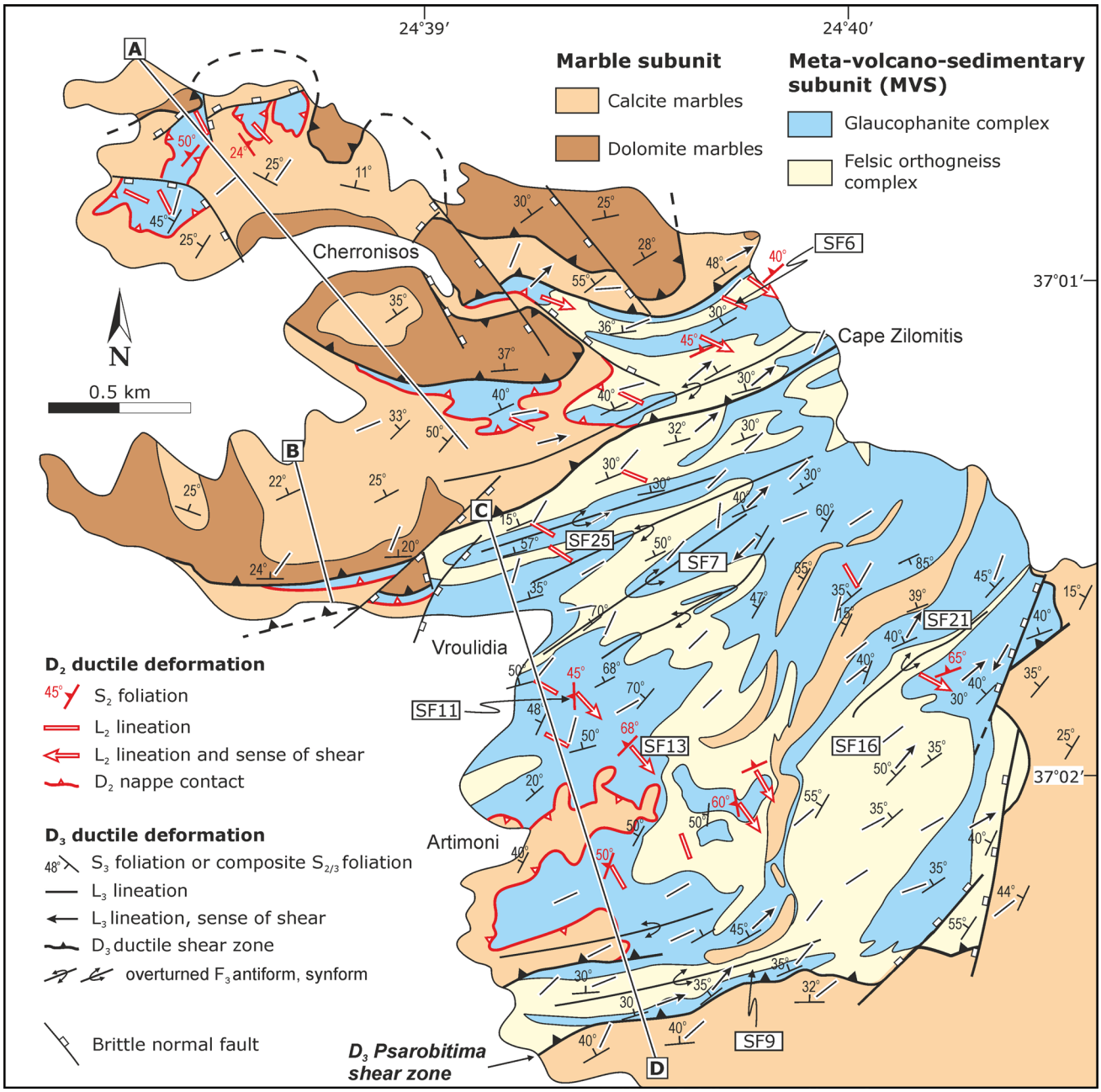

Fig. 2 New geological/structural map of the northern part of Sifnos Island showing the major rock subunits and the structural elements of the recognized deformation phases in the map area. Lettered section *A–D* refers to the composite cross section in Fig. 3. Locations of samples (SF6, 7, 9, 11, 13, 16, 21, 25) used for chemical analysis are also shown

preserved in garnet porphyroblasts, in the form of an internal foliation defined by the orientation of inclusion trails (see also Lister and Raouzaios 1996). Our microstructural observations show that the inclusion trails in garnets are defined by glaucophane, epidote and mica and quartz and are commonly straight and oblique to the matrix S_2 foliation (Fig. 6a, b), revealing intertectonic (in the sense of Passchier and Trouw 2005) garnet growth with respect to D_1 and D_2 deformation. Few garnets display an internal foliation slightly curved at the rims (Fig. 6c), which implies that these crystals were possibly syntectonic with respect to D_2, at least during the last stages of their growth.

The D_2 deformation is mainly expressed by a homogeneously developed mylonitic foliation which is defined by the shape preferred orientation of diagnostic minerals of eclogite-/blueschist-facies metamorphism (garnet, omphacite, sodic amphibole, paragonite). S_2 is commonly parallel to the metamorphic/compositional layering, marked, for example,

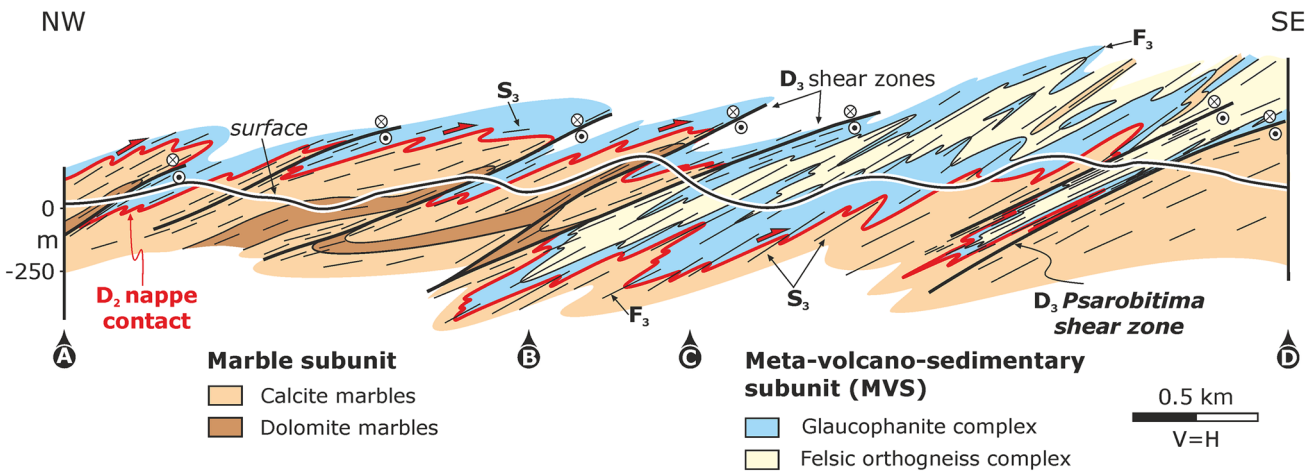

Fig. 3 Composite cross section (*a–d*) depicting the internal structural architecture of the CBU in north Sifnos; for location, see Fig. 2

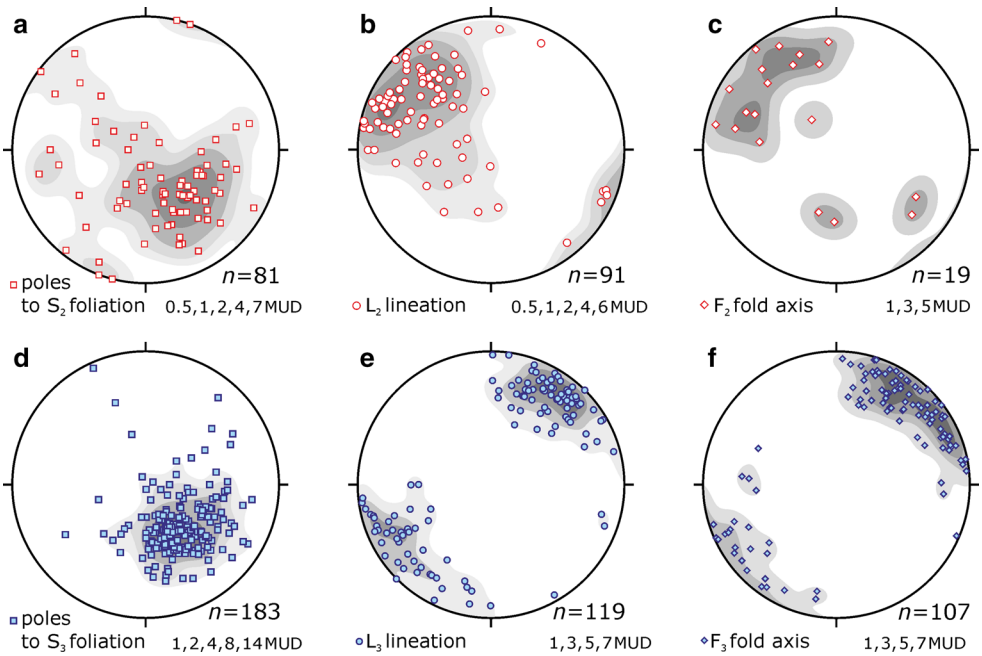

Fig. 4 Stereoplots (lower hemisphere—equal-area projections) of structural data collected from both the metavolcano-sedimentary (MVS) and Marble subunits showing **a** S_2 foliation, **b** L_2 lineation, **c** F_2 fold axis, **d** S_3 foliation, **e** L_3 lineation and **f** F_3 fold axis. *MUD* multiples of uniform distribution

by alternating eclogite and glaucophanite bands as well as by intercalated garnet-rich and garnet-poor layers. The S_2 typically dips moderately toward northwest (Fig. 4a). Within the foliation plane, a pronounced mineral-stretching lineation (L_2) plunges gently toward the northwest to west-northwest with a mean trending 304° (Fig. 4b). The latter could represent the direction of maximum finite elongation caused by D_2. It is emphasized that the L_2 orientation was selectively measured in domains where D_2 fabrics are unaffected or only slightly affected by the subsequent folding phase. The L_2 is easily recognized in the field by the parallel alignment of columnar and acicular sodic amphibole grains, which typically have a high aspect ratio. However, there are also examples where the sodic amphiboles exhibit a moderate-to-weak shape preferred orientation on S_2 planes. In such cases, some sodic amphibole grains lie oblique to L_2, while the majority of the grains are broken and extended parallel to the L_2 orientation. This microstructural feature implies that several of the sodic amphibole grains pre-date D_2 (could be related to D_1) and/or grew during early D_2 stages, and the progressive D_2 deformation caused mechanical rotation of grains into parallelism with the L_2 stretching direction. This NW–SE-oriented ductile stretching also causes boudinaging of S_2 foliation forming decimeter-scale pinch-and-swell structures. The F_2 fold hinges lie subparallel or at small angles to the L_2 (Fig. 4c). These isoclinal F_2 folds, which occur sporadically in the map area, display a purely similar geometry with acute shape (Fig. 5a, b).

Evidence for D_2 deformation was mainly found at the lower structural levels of the MVS subunit close to the contact with the underlying marble in Cherronisos and Artimoni areas (Fig. 2). In these areas, the D_2 deformation fabrics are very intensely developed, suggesting that the contact between the MVS and the Marble subunit marks a syn-metamorphic D_2 ductile shear zone (Figs. 3, 5c). This shear zone is interpreted as a thrust sense shear zone inasmuch as it juxtaposes metaigneous rocks over pure marbles, an association that is not likely to be primary (see Keiter et al. 2004 for a similar interpretation in Syros). Evidence for the sense of shear during D_2 deformation is generally scarce at the outcrop scale due to absence of kinematic indicators. In turn, several microscopic shear sense indicators such as σ- and δ-structures around garnet porphyroclasts (Fig. 6a–c), shear bands and sigmoid lenses (Fig. 6d) were recognized in thin sections oriented parallel to L_2 and perpendicular to S_2. These shear sense indicators indicate a consistent top-to-the-SE sense of shear during D_2 nappe emplacement.

Fig. 5 Field photographs showing the structural features of all deformation phases. **a** Refolding of an early F_2 isoclinal fold by gently inclined F_3 fold in MVS subunit (Artimoni area). On limbs of F_2 appears a composite $S_{1/2}$ foliation, which is parallel to the F_2 axial planes. **b** Refolding of an early F_2 isoclinal fold by gently inclined F_3 fold in Marble subunit (Cherronisos area). **c** Oblique air photograph showing the D_2 thrust contact, which carries the MVS over the Marble subunit, and subsequent D_3 ductile thrust, which restacks the early nappe pile bringing the structurally lower Marble subunit over the MVS subunit (north side of Vroulidia bay); field of view is 300 m wide. **d** Typical mesoscopic F_3 fold with Z-asymmetry that deforms the MVS subunit rocks, i.e., glaucophanites (*blue*) and eclogites (*green*). The composite $S_{2/3}$ foliation on long limbs of F_3 fold is subparallel to axial planar foliation (S_3) (Road cut section 1 km east from Vroulidia bay). **e** Typical mesoscopic F_3 fold with S-asymmetry observed in felsic orthogneisses (*light brown*) and glaucophanites (*blue*) of MVS subunit (Road cut section 1.2 km east from Vroulidia bay). **f** Map-scale F_3 fold deforming glaucophanites and felsic orthogneisses of the MVS subunit. A composite foliation $S_{2/3}$ appears to be subparallel to the long limb of F_3 fold. (Vroulidia area); field of view is 215 m wide. **g** Glaucophanite (*dark*) and felsic orthogneiss (*white*) D_3 mylonites (Road cut section 500 m west from Cape Zilomitis); notebook for scale. **h** View of the Psarobitima ductile shear zone (D_3) located at the deeper structural levels of the study area; field of view is 200 m wide

D_3 deformation phase: nappe restacking and refolding

The ductile D_3 deformation forms the dominant structures throughout much of the study area. A main D_3 deformation feature observed at outcrop scale is a gentle to moderate NW-dipping planar fabric, S_3, which disrupts and often transposes all earlier D_1–D_2 fabrics (Figs. 2, 4d, 5d, e). The S_3 is heterogeneously developed and varies in intensity from a spaced cleavage to a mylonitic foliation. It is commonly defined by flattened mineral aggregates (e.g., quartz and calcite) as well as by pervasive alignment of sodic amphibole, epidote, white mica and occasionally chlorite flakes. Developed within the plane of S_3 is a NE-trending mineral-stretching lineation, L_3 (Figs. 2, 4e). L_3 is typically defined by the shape preferred orientation of sodic amphibole and epidote columnar crystals in rocks of the MVS subunit and streaks of mica in impure calcite marble.

The S_3 foliation is commonly axial planar to outcrop- and map-scale cylindrical F_3 folds, which vary in style from gently inclined to recumbent, and in tightness from open to isoclinal, although the majority is characterized by close or tight geometry (Figs. 2, 3, 5a, b, d–f). F_3 fold axes are concentrated on the NE and SW quadrants on the equal-area nets, subparallel or at small angles to the L_3 lineation (Fig. 4f). Field observations showed that several mesoscopic open F_3 folds are oriented subparallel to L_3 as well as several isoclinal F_3 folds are oriented oblique to L_3. This reveals that the angle of obliquity between the F_3 hinge lines and L_3 lineation seems not to depend on the interlimb angle.

Map-scale F_3 folds have distinct patterns of long limb–short limb asymmetry and consistently display a Z-shaped geometry when they viewed toward the northeast showing SE vergence (Fig. 3). Mesoscopic F_3 folds commonly occur as second-order parasitic folds to map-scale folds, and their vergence is related to their position on the associated first-order fold structures. Parasitic F_3 folds exhibit Z-asymmetry (SE vergence) on long limbs and S-asymmetry (NW-vergence) on the short limbs of the map-scale folds (Fig. 5d, e). In many instances, the long limb of mesoscopic F_3 folds tends to be thinner compared to broader short limb. The axial planar foliation (S_3) does not bisect the interlimb angle but is subparallel to the long limb (Fig. 5d, f). However, the intersection between the S_2 and S_3 planes is parallel to fold hinges. The S_3 clearly transposes the S_2 foliation within F_3 hinge zones and on short limbs, but the degree of transposition varies spatially and depends on the intensity of D_3 deformation. On long limbs of many F_3 folds, both S_2 and S_3 are indistinguishable from one another due to their coplanarity and therefore are considered to form a composite $S_{2/3}$ foliation. Within such composite $S_{2/3}$ foliation planes, the L_3 lineation is commonly recognized, revealing that the early S_2 foliation has been reused by D_3 deformation. Note that the term "re-use" as defined by Davis (1995) "refers to the accommodation of progressive strain by pre-existing foliations during a subsequent deformation." Moreover, there are also several examples where $S_{2/3}$ planes bear both the L_2 (NW-trending) and L_3 (NE-trending) lineation (Fig. 2). The degree of preservation of L_2 and development of L_3 lineation vary spatially and primarily depend on the intensity of D_3 deformation.

Strain during D_3 phase is heterogeneous and commonly localized into ductile shear zones of varying scales. Structural mapping showed that D_3 shear zones cut across the axial plane or cut out the inverted short limb of F_3 folds (Fig. 3). We have mapped a series of discrete, major D_3

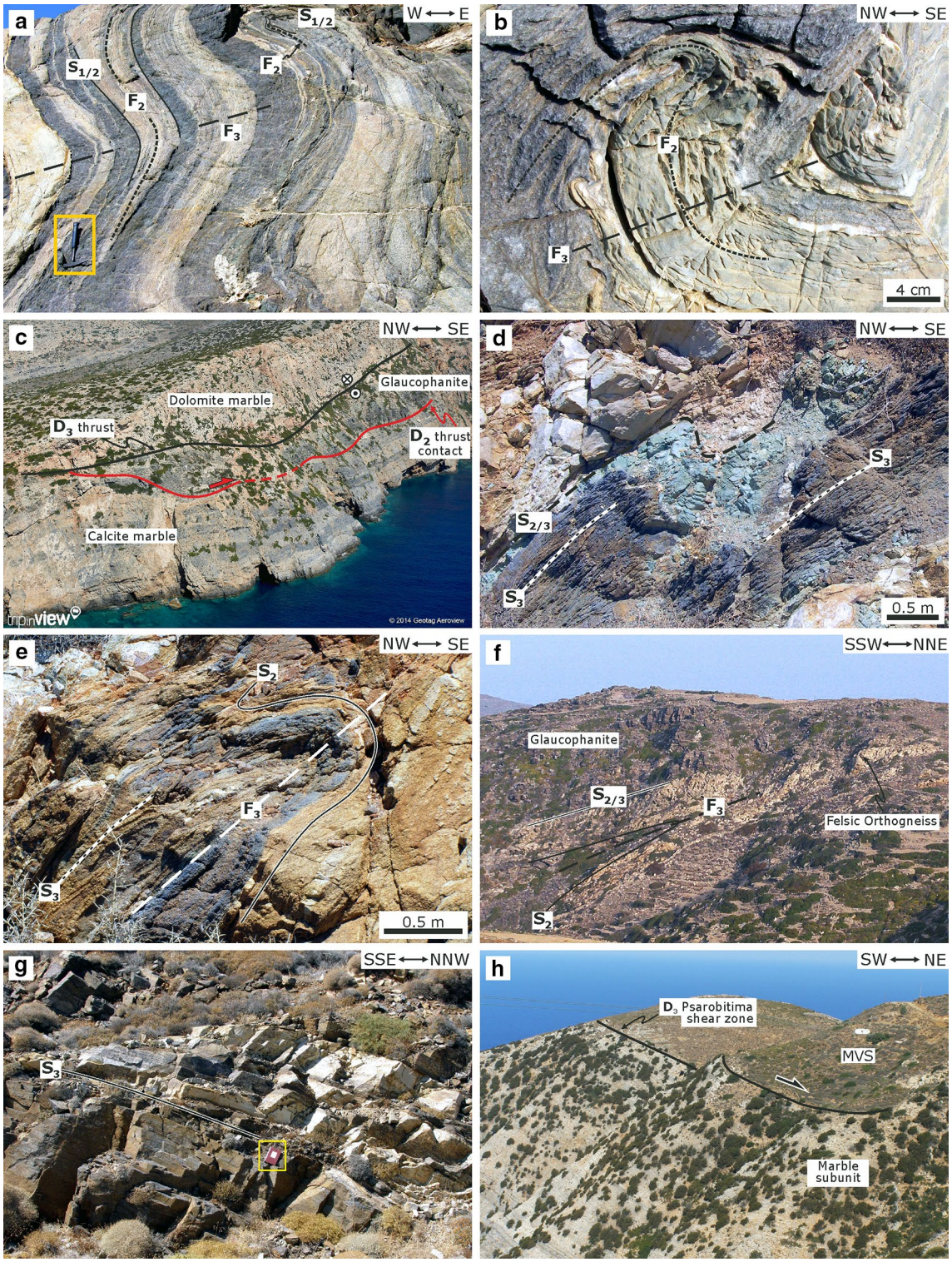

shear zones, presented in Figs. 2 and 3. The D_3 shear zones carry the Marble subunit over the MVS subunit, transposing the nappe contact developed during D_2 phase (Fig. 5b). These major D_3 shear zones are marked by mylonitic panels few tens of meters thick. Mylonitic zones are characterized by a single foliation (S_3) and lineation (L_3), and in individual outcrops commonly display shape fabrics indicative of S = L or S > L tectonites (Fig. 5g). Locally, some relict and dismembered isoclinal folds with attenuated limbs are observed within D_3 mylonitic zones which pass diffusely to broad domains of lower strain where tight F_3 folds are typical.

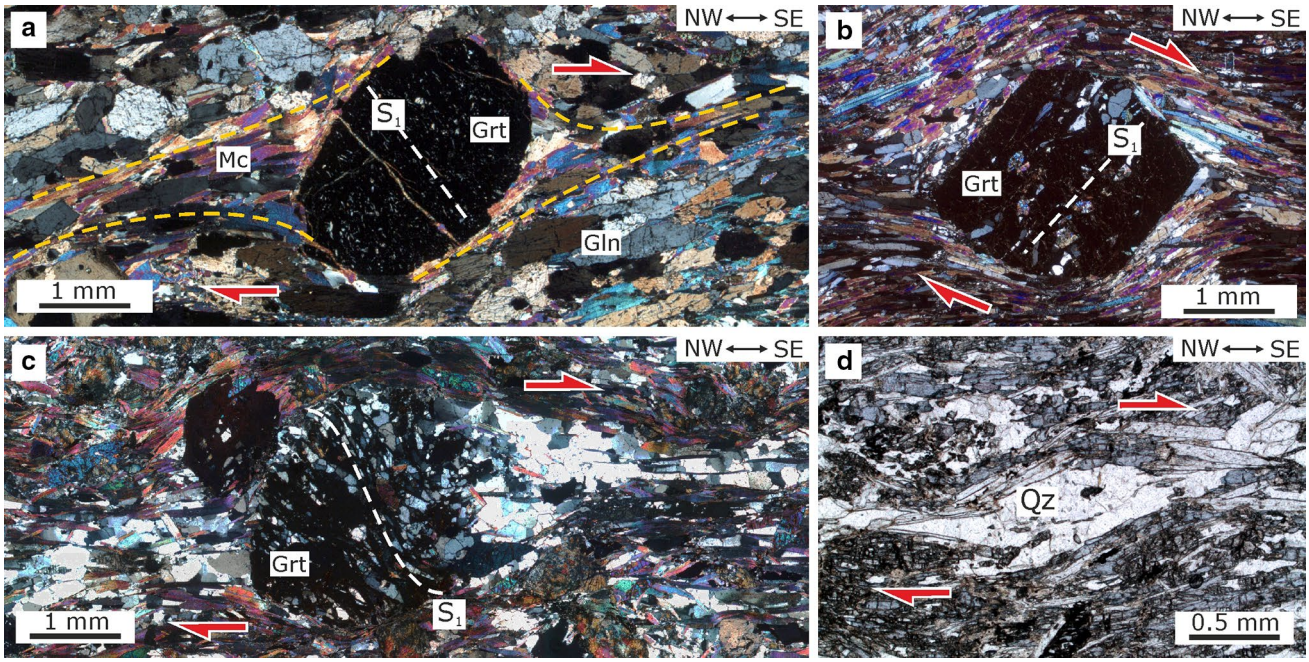

Fig. 6 Photomicrographs of microstructures and kinematic indicators of D_2 deformation. All sections are oriented parallel to L_2 lineation and normal to S_2 foliation. **a** δ-Type garnet porphyroclast with straight inclusion trails (S_1) oblique to the matrix S_2 foliation in a glaucophanite; crossed-polarized light. **b** σ-Type garnet porphyroclast with straight inclusion trails (S_1) oblique to the matrix S_2 foliation in a glaucophanite; crossed-polarized light. **c** σ-Type garnet porphyroclast, with internal foliation slightly curved at the rims, indicating syn-tectonic growth at the late stages of D_2 (glaucophane schist); crossed-polarized light. **d** Sigmoid quartz lense embedded in a blue amphibole-rich matrix (felsic orthogneiss); plane-polarized light. Asymmetry of kinematic indicators, in all photomicrographs, indicates top-to-the-SE sense of shear. Abbreviations of minerals: Gln, Glaucophane; Grt, Garnet; Mc, Mica; Qz, Quartz

In all D_3 shear zones, both S_3 and L_3 fabrics are defined by the shape preferred orientation of macroscopically visible, lenticular blue amphibole grains. This reveals that mylonitization occurred or at least commenced under HP conditions. With the exception of a major shear zone located at the southern part of the map area (Psarobitima area; Figs. 2, 3, 5h), D_3 mylonites show no or little signs of retrogression to greenschist-facies conditions. This is manifested by the presence of well-preserved blue amphibole grains and the absence of indicative retrograde minerals such as chlorite and calcic amphiboles parallel to S_3 fabrics. In Psarobitima shear zone, which is defined by ca. 50 m thick mylonites of both Marble and MVS subunits, the earlier D_2 nappe contact is completely transposed due to intense D_3 deformation. Here, there are many foliation (S_3) parallel bands of extensive growth of retrograde mineral assemblages expressed mainly by the partial replacement of blue amphibole by albite, chlorite and epidote (see also next section). A static overgrowth of chlorite locally occurs but is of minor extent.

Analysis of D_3 kinematics was focused on major mylonitic shear zones. In these zones, a variety of mesoscopic and microscopic shear sense indicators such as σ- and δ-type porphyroclasts, S/C structures, asymmetric boudins, domino-type fragmented clasts and mica fish are recognized in mylonitized rocks of the Marble and MVS subunits (Figs. 2, 7a–f). The majority of these asymmetric indicators indicate a top-to-the-NE sense of movement. Domains of lower D_3 strain, which display a well-developed D_3 foliation, are often characterized by coaxial structures and kinematic indicators that record conflicting shear sense within a single outcrop or lack of clear sense of shear (Fig. 2).

Amphibole composition and deformation fabrics

Eight representative samples from MVS subunit were selected in order to investigate the composition and the potential chemical zoning of amphiboles that define the D_2 and D_3 fabrics (i.e., foliation and lineation). The purpose of this analysis is to understand whether the syn-kinematic growth of amphiboles in different stretching directions is linked with prograde or retrograde metamorphism. The suite of samples includes one glaucophanitic eclogite (SF25), three glaucophanites (SF6, SF9, SF13), two glaucophane schists (SF11, SF21) and two amphibole-bearing felsic orthogneisses (SF7, SF16). In terms of deformation fabrics, all samples display a single, penetrative, in part mylonitic foliation (S_2 or S_3) and bear a well-developed L_2 (samples SF6, 11, 13, 25) or L_3 (samples SF7, 9, 16, 21) stretching lineation defined by the strong shape preferred

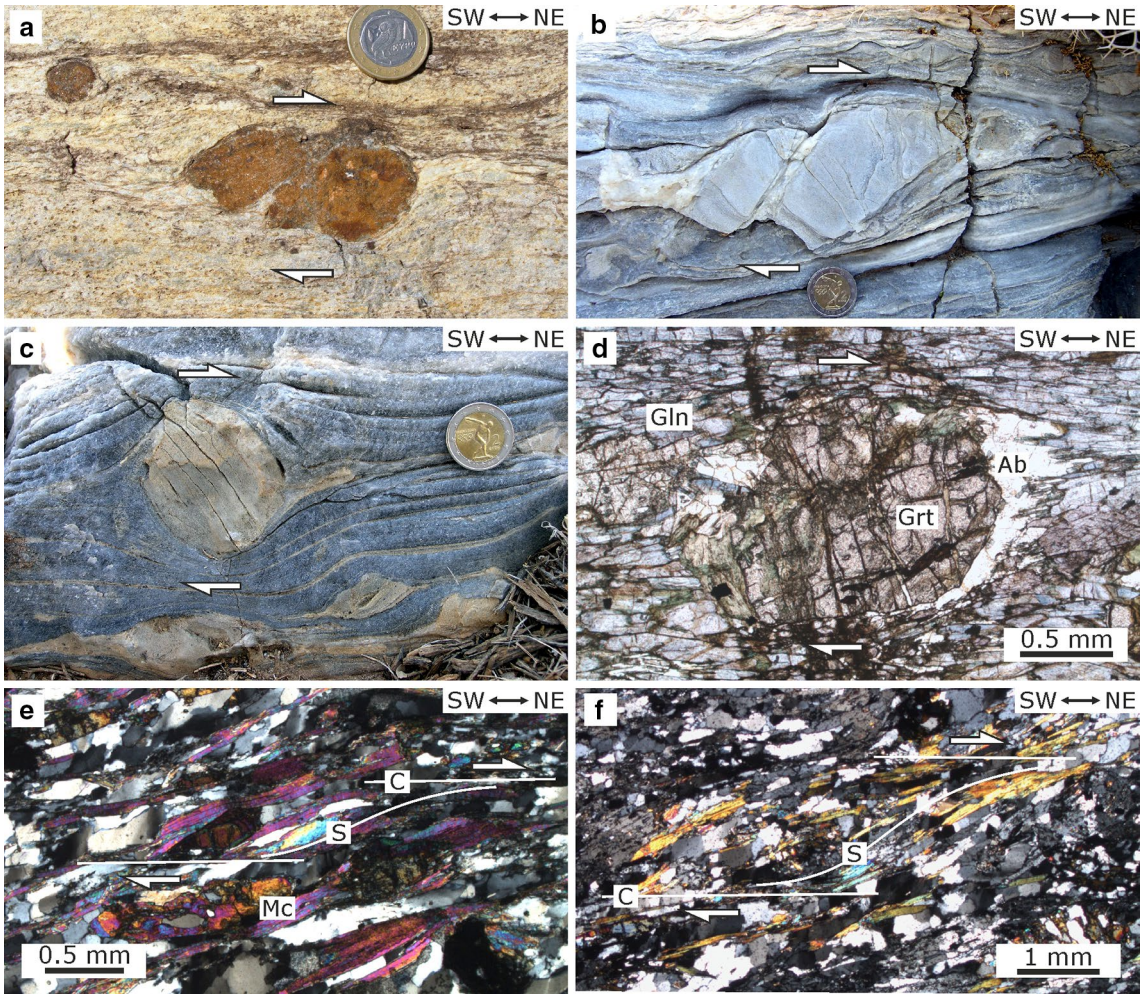

Fig. 7 Photographs of meso- and microscopic kinematic indicators for D_3 deformation phase observed in the Marble and MVS subunits. **a** Mesoscopic σ-type garnet porphyroclast with asymmetric strain *shadows* indicating top-to-the-NE sense of shear; coin for scale (felsic orthogneiss). **b** Mesoscopic domino-type fragmented dolomitic clast embedded in mylonitic calcite marble indicating top-to-the-NE sense of shear; coin for scale. **c** δ-Type dolomitic clast embedded in mylonitic calcite marble indicating top-to-the-NE sense of shear; coin for scale. **d** Photomicrograph (plane-polarized light) of σ-type garnet porphyroclast indicating top-to-the-NE sense of shear. The asymmetric strain shadows is consist of albite (Ab), which partially replaces glaucophane (glaucophane schist). **e**, **f** Photomicrographs (crossed-polarized light) of S/C fabrics in quartz-mica schist indicating top-to-the-NE sense of shear

orientation of amphibole needles (Fig. 8). The position of each sample is shown in the geological map of Fig. 2, while the geographic coordinates of each sample locality are given in supplementary material.

Analytical techniques

Analyses of samples were made on polished thin sections cut parallel to lineation and normal to foliation. The chemical compositions of amphiboles were determined using a JEOL-6300 Scanning Electron Microscope at the University of Patras, under operating conditions of 20 kV accelerating voltage, 10 nA beam current and 3–5 μm beam diameter. Natural and synthetic standards were used for calibration, while the measured values were corrected employing the ZAF method. Amphibole formulae were calculated considering the general formula $A_{0-1}X_2Y_5Z_8O_{22}(OH)_2$ (A and X: Ca, Na, K; Y: Fe^{+2}, Fe^{+3}, Al, Mg, Mn and Ti, all octahedrally coordinated; Z: Al and Si, tetrahedrally coordinated) for 13 cations in the Y and X sites following the procedure recommended by Schumacher in Leake et al. (1997). Amphibole classification is based on the nomenclatures of Leake et al. (1997). Representative scanning electron microscope–wavelength dispersive spectroscopy (SEM–WDS) analyses are given in Table 1.

Amphiboles defining D_2 fabrics

Blue amphiboles that define D_2 fabrics occur as idioblastic or subidioblastic grains and are characterized, in lineation

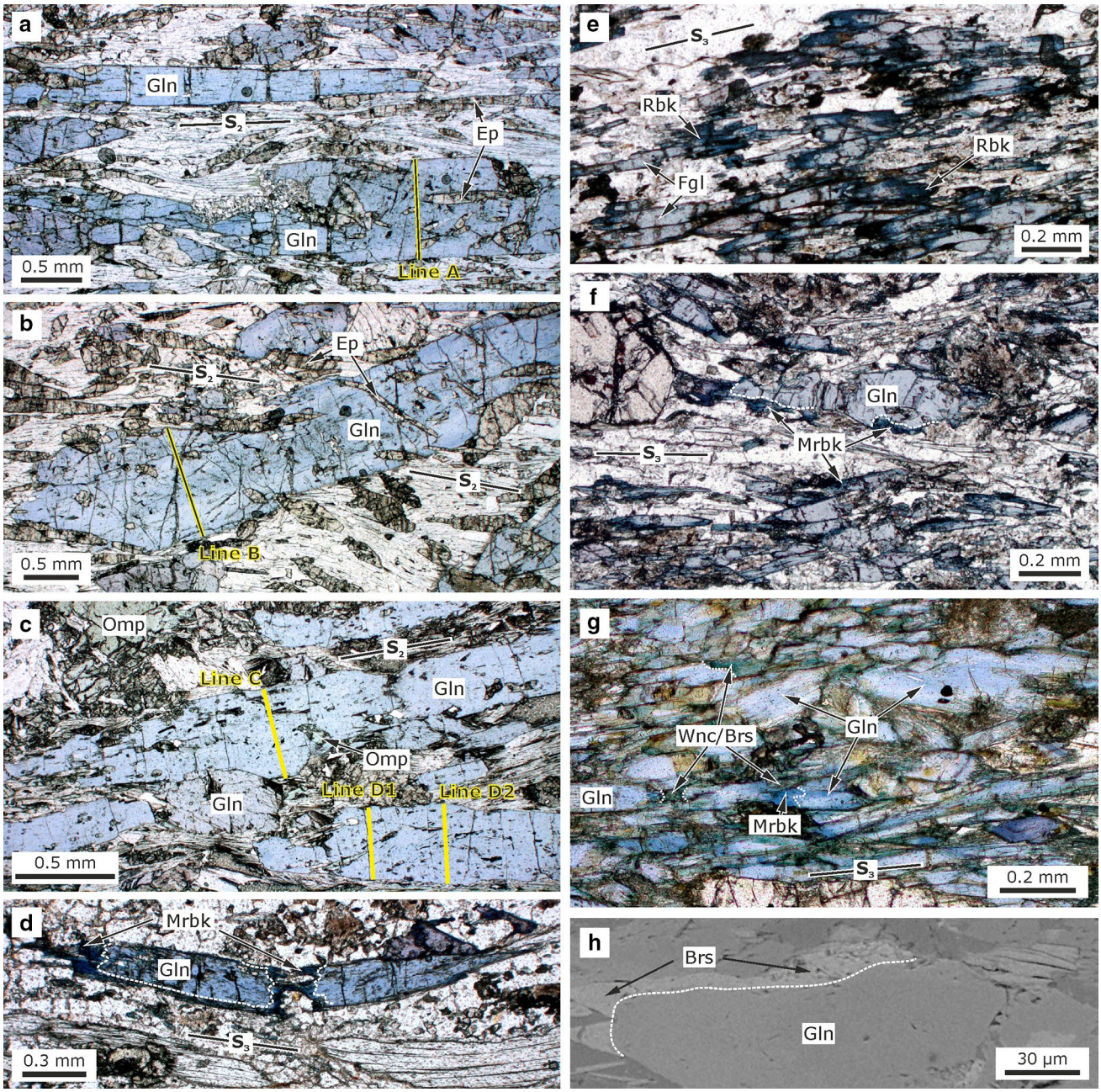

Fig. 8 **a** Photomicrograph (plane-polarized light) of sample SF11 showing glaucophane (Gln) and epidote (Ep) crystals which growth parallel to S_2 foliation. *Line A* shows the path of plot in Fig. 9f. **b** Photomicrograph (plane-polarized light) of sample SF11 showing a large acicular blue amphibole grain which is oblique to S_2 foliation. *Line B* shows the path of plot in Fig. 9f. **c** Photomicrograph (plane-polarized light) of sample SF25 showing glaucophane (Gln) crystals which growth parallel or subparallel to S_2 foliation. *Lines C*, *D1*, *D2* show the paths of plots in Fig. 9g. **d** Photomicrograph (plane-polarized light) of sample SF7 showing zoned boudinaged sodic amphibole defining S_3 foliation. **e** Photomicrograph (plane-polarized light) of sample SF16 showing zoned sodic amphiboles which growth parallel to S_3 foliation. **f** Photomicrograph (plane-polarized light) of sample SF21 showing glaucophane (Gln) grain which growth parallel to S_3 foliation and is rimed by magnesioriebeckite (Mrbk). **g** Photomicrograph (plane-polarized light) of sample SF9 showing fractured sodic amphiboles grains define S_3 foliation. Winchite (Wnc) and barroisite (Brs) growth at the necks of glaucophane grains. **h** Backscattered electron microscope image of sample SF9 showing glaucophane crystal rimed by barroisite (Brs). Geographic coordinates of samples are given in Table A1. Abbreviations of minerals: Fgl, ferro-glaucophane; Omp, omphacite; Rbk, riebeckite

parallel and foliation normal sections, by mean aspect ratio (a/b) of 6.8 and mean grain size [$(ab)^{½}$] of 700 µm, where a and b are the lengths of the long and short axis of a grain, respectively (Fig. 8a–c). Some amphibole grains are fractured perpendicular to their long axis, forming microboudin structures. Although the vast majority of

Table 1 Representative chemical analyses of amphibole crystals

Mineral[a] Occurrence	SF6		SF11		SF13		SF25		SF7		SF9		SF16		SF21	
	Gln core	Gln rim	Gln core	Gln rim	Gln core	Gln rim	Gln core	Gln rim	Gln core	Mrbk neck	Gln core	Brs neck	Fgl core	Rbk rim	Gln core	Mrbk rim
Oxides (wt%)																
SiO_2	57.30	57.70	56.43	57.83	56.83	57.89	56.91	57.23	57.35	55.05	57.06	50.95	56.71	54.08	56.94	55.34
TiO_2	0.00	0.00	0.00	0.00	0.00	0.00	0.00	0.00	0.00	0.00	0.00	0.00	0.00	0.00	0.00	0.00
$Al2O_3$	10.98	10.10	10.56	10.55	11.55	11.45	10.43	11.43	11.40	2.88	10.51	4.74	10.25	4.51	11.48	6.18
FeO	9.36	10.62	10.55	11.94	13.03	10.94	12.82	10.87	13.61	23.26	12.43	21.05	16.24	25.64	13.20	19.59
MnO	0.00	0.00	0.00	0.00	0.00	0.00	0.00	0.00	0.00	0.00	0.00	0.00	0.00	0.00	0.00	0.00
MgO	11.54	10.90	12.18	9.55	8.18	9.39	10.21	9.39	8.14	8.34	8.83	9.62	6.80	5.34	8.69	8.43
CaO	1.15	1.15	1.60	0.20	0.00	0.40	1.53	0.68	0.18	2.97	0.00	9.37	0.22	2.05	0.67	1.62
Na_2O	6.98	6.91	6.74	7.54	7.34	7.25	6.74	7.21	7.43	5.65	7.42	1.82	7.37	5.96	7.39	6.42
K_2O	0.00	0.00	0.00	0.00	0.00	0.00	0.00	0.00	0.00	0.00	0.00	0.00	0.00	0.00	0.00	0.00
Total	97.31	97.38	98.05	97.61	96.93	97.32	98.64	96.81	98.11	98.15	96.25	97.54	97.59	97.58	98.38	97.58
Cations (assuming 23 O; recalculation based on 13eCNK)																
Si	7.82	7.92	7.65	7.96	7.90	7.96	7.78	7.93	7.91	7.92	7.98	7.49	7.97	7.92	7.84	7.86
Al^{IV}	0.18	0.08	0.35	0.04	0.10	0.04	0.22	0.07	0.09	0.08	0.02	0.51	0.03	0.08	0.16	0.14
Al^{VI}	1.58	1.55	1.34	1.67	1.79	1.82	1.46	1.80	1.76	0.41	1.71	0.31	1.67	0.70	1.70	0.89
Ti	0.00	0.00	0.00	0.00	0.00	0.00	0.00	0.00	0.00	0.00	0.00	0.00	0.00	0.00	0.00	0.00
Fe^{+3}	0.41	0.35	0.77	0.30	0.33	0.17	0.54	0.13	0.30	1.18	0.31	0.74	0.29	1.05	0.30	0.99
Fe^{+2}	0.65	0.87	0.43	1.07	1.18	1.09	0.93	1.13	1.27	1.63	1.15	1.85	1.62	2.09	1.22	1.33
Mn	0.00	0.00	0.00	0.00	0.00	0.00	0.00	0.00	0.00	0.00	0.00	0.00	0.00	0.00	0.00	0.00
Mg	2.35	2.23	2.46	1.96	1.69	1.93	2.08	1.94	1.67	1.79	1.84	2.11	1.43	1.17	1.78	1.78
Ca	0.17	0.17	0.23	0.03	0.00	0.06	0.22	0.10	0.03	0.46	0.00	1.48	0.03	0.32	0.10	0.25
Na_B	1.83	1.83	1.77	1.97	1.98	1.93	1.77	1.90	1.97	1.54	2.00	0.52	1.97	1.68	1.90	1.75
Na_A	0.02	0.01	0.00	0.04	0.00	0.00	0.01	0.04	0.01	0.03	0.01	0.00	0.04	0.02	0.07	0.01
K	0.00	0.00	0.00	0.00	0.000	0.00	0.00	0.00	0.00	0.00	0.00	0.00	0.00	0.00	0.00	0.00
Total	15.02	15.01	15.00	15.04	14.98	14.99	15.01	15.04	15.01	15.03	15.01	14.99	15.04	15.02	15.07	15.01

Brs, barroisite; Fgl, ferroglaucophane; Gln, glaucophane; Mrbk, magnesioriebeckite; Rbk, riebeckite

[a] The classification of amphiboles is based on Leake et al. (1997)

amphiboles are aligned parallel to S_2 foliation, there are few grains, often with large grain size, that lie at small angle to the trace of S_2 (Fig. 8b). This microstructural feature implies that grains were grown oblique to S_2 and progressively rotated toward parallelism with foliation during D_2 deformation. In the analyzed samples, the D_2 fabrics are also defined by the shape preferred orientation of white mica, omphacite and occasionally epidote (Fig. 8a–c). These mineral phases also occur as inclusions in amphibole grains (Fig. 8a–c).

All analyzed blue amphiboles have the chemical composition of glaucophane sensu stricto and Na_B content higher than 1.7 pfu (Fig. 9a; Table 1). The X_{Mg} [=Mg/(Mg + Fe^{+2})] generally varies from 0.5 to 0.85 and $X_{Fe^{+3}}$ [=Fe^{+3}/(Fe^{+3} + Al^{VI})] from 0 to 0.4 (Fig. 9a). Glaucophane grains in sample SF6 show fairly narrow ranges of both X_{Mg} and $X_{Fe^{+3}}$ values compared to the other three samples, while the observed variation of X_{Mg} and $X_{Fe^{+3}}$ values in sample SF13 seems to be irregular (Fig. 9b, c). In turn, a weak internal chemical zonation is detectable in glaucophane grains of two samples (SF11, SF25). This zonation is mainly expressed by a general decrease in $X_{Fe^{+3}}$ values from cores to rims across the long axes of individual grains (Fig. 9d, e; Table 1). It is worth noting that this trend toward lower $X_{Fe^{+3}}$ values has been recorded both in grains oriented parallel to S_2 foliation and grains slightly oblique to S_2. Analyses also showed variation in Na_B content across the glaucophane grains in samples SF11 and SF25 (Fig. 9f, g). Specifically, in sample SF11, Na_B systematically increases from ca. 1.75 pfu in the core to ca. 2.0 pfu in the rim of two large glaucophane grains oriented parallel (Figs. 8a, 9f; Line A) and slightly oblique (Figs. 8b, 9f; Line B) to S_2 foliation, respectively. A similar but less pronounced trend toward higher Na_B contents in rims is recorded in two glaucophane grains in sample SF25 (Figs. 8c, 9g).

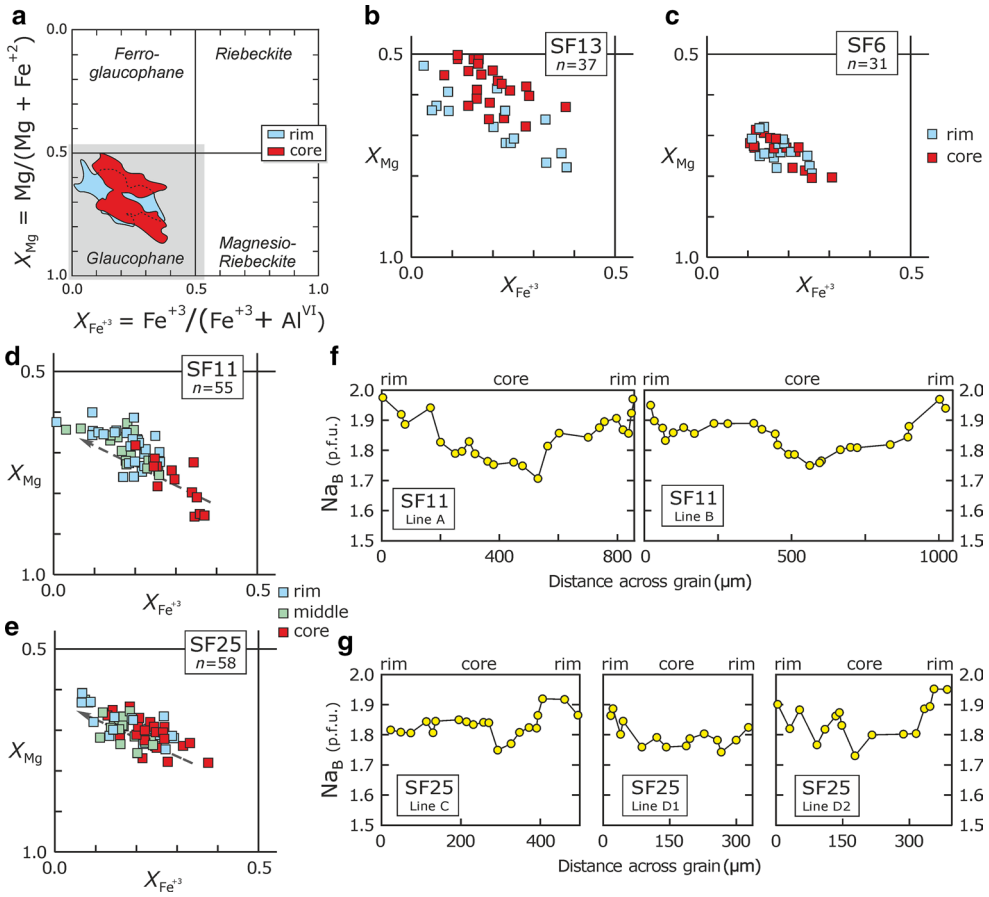

Fig. 9 Plots of sodic amphiboles composition defining D_2 fabrics. **a** Summarizing X_{Mg} versus $X_{Fe^{+3}}$ plot that shows the composition of cores and rims of all analyzed amphibole grains. **b** X_{Mg} versus $X_{Fe^{+3}}$ plot showing the composition of sodic amphibole grain in sample SF13. **c** X_{Mg} versus $X_{Fe^{+3}}$ plot showing the composition of sodic amphibole grain in sample SF6. **d** X_{Mg} versus $X_{Fe^{+3}}$ plot showing the composition of sodic amphibole grain in sample SF11. **e** X_{Mg} versus $X_{Fe^{+3}}$ plot showing the composition of sodic amphibole grain in sample SF25. **f**, **g** Variation in Na_B content across representative sodic amphibole grains in samples SF11 and SF25, respectively; the location of analyzed lines A, B, C, D1 and D2 is shown in Fig. 8a–c. The structural position of samples is shown in Fig. 2, while geographic coordinates of each sample are given in Table A1

Summarizing, acicular blue amphibole grains that define D_2 fabrics have a pure glaucophane composition. The recorded decrease in $X_{Fe^{+3}}$ values coupled with increase in Na_B content toward the rims of some grains implies increase in metamorphic pressure (e.g., Brown 1977; Laird and Albee 1981) during the syn-kinematic growth of glaucophane.

Amphiboles defining D_3 fabrics

Blue amphibole grains that define D_3 fabrics are characterized by mean aspect ratio of 7.3 and mean grain size 180 μm. Commonly, the amphibole needles are stretched and necked forming microboudins parallel to L_3 and the trace of S_3. The majority of blue amphiboles in felsic orthogneiss (SF7, 16) and glaucophane schist (SF21) samples display an optical zoning expressed by light blue cores and thin, often discontinuous deep blue rims and/or edges (Fig. 8d–f). A similar but less pronounced optical zoning is observed in a glaucophanite sample (SF9; Fig. 8g). The amphibole cores consist of glaucophane (X_{Mg} < 0.7; samples SF7, 9, 21) or ferroglaucophane (X_{Mg} > 0.35; sample SF16) with $X_{Fe^{+3}}$ less than 0.3 and Na_B content typically higher than 1.85 pfu (Fig. 10; Table 1). It is worth noting that glaucophane cores are chemically identical with glaucophane grains defining D_2 fabrics (Figs. 9, 10). Rims and edges are commonly composed of (ferro-) glaucophane with $X_{Fe^{+3}}$ higher than 0.3 or (magnesio-) riebeckite with $X_{Fe^{+3}}$ between 0.5 and 0.85, while Na_B content varies from 1.8 to 1.5 pfu (Fig. 10; Table 1). In felsic orthogneiss (magnesio-) riebeckite also occurs as discrete, isolated needles with small grain size. In the glaucophanite sample, the rims, edges and necks of Na amphibole are also syn-kinematically overgrown by Ca–Na amphibole with composition at the border line between winchite and barroisite (Fig. 8g,

h). Na_B content of Ca–Na amphiboles is low and ranges between 0.5 and 0.6 pfu (Table 1).

Summarizing, the analyzed Na amphiboles defining D_3 fabrics are characterized by a systematic increase in $X_{Fe^{+3}}$ values and decrease in Na_B content from the cores to rims and locally are overgrown by Ca–Na amphibole. This zoning pattern reflects decompression during amphibole growth (Brown 1977; Laird and Albee 1981). During progressive D_3 deformation, rocks passed from the stability field of glaucophane (e.g., Carman and Gilbert 1983; Evans 1990) to the stability field of winchite/barroisite (Otsuki and Banno 1990). Moreover, we can assume that D_3 amphiboles resulted from dynamic recrystallization of D_2 amphiboles and subsequently developed the above-described chemical zoning, based on that: (a) The amphiboles defining D_3 fabrics are much smaller than those defining D_2 fabrics, and (b) the cores of D_3 amphiboles are chemically identical to D_2 amphiboles.

Comparison with previous analyses

Previous petrological works (Okrusch and Bröcker 1990; Groppo et al. 2009) in north Sifnos have shown that sodic amphibole grains occurring in eclogites, glaucophanites and glaucophane schists typically have the chemical composition of glaucophane sensu stricto with X_{Mg} between 0.5 and 0.8, and $X_{Fe^{+3}}$ lower than 0.3. In same lithologies, we have recorded similar glaucophane composition for sodic amphiboles, which are oriented parallel to L_2 lineation or occupy the cores of grains that oriented parallel to L_3 lineation (Figs. 9a, 10). Also, microprobe analyses by Okrusch and Bröcker (1990) and Groppo et al. (2009) have revealed that sodic amphiboles in quartzites commonly have a riebeckite composition with X_{Mg} between 0.3 and 0.5. Our analyses shown that (magnesio-) riebeckite also occurs as discrete and isolated needles in quartz-rich felsic orthogneisses. It should be noted that (magnesio-) riebeckite can also occur at the rims of sodic amphibole grains defining L_3 in all rock types. Sodic amphibole grains rimmed by winchite/barroisite in quartzites have been described by Groppo et al. (2009). A similar chemical zoning recognized in one of our glaucophanite samples (Fig. 10).

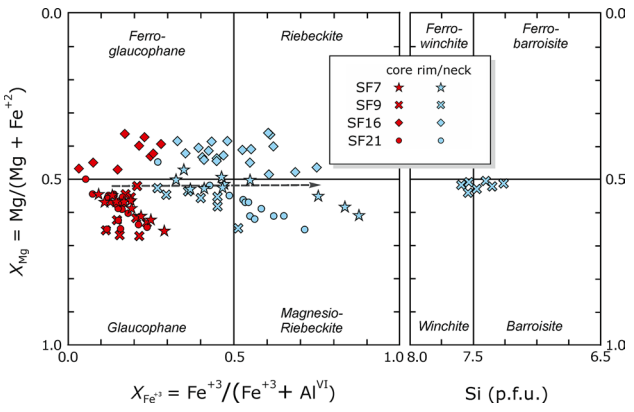

Fig. 10 Plots of sodic amphibole composition defining D_3 fabrics. The structural position of samples is shown in Fig. 2, while geographic coordinates of each sample are given in Table A1

Discussion

Synthesis

Restoration of the nappe stack recorded in north Sifnos (Fig. 3) reveals a pre-D_2 tectonostratigraphic succession in which either the MVS subunit is overlain by the Marble subunit or the MVS and Marble subunits have a lateral relationship. Although it is difficult to draw a safe conclusion, it seems that the first possibility (Fig. 11a) is more plausible since a similar tectonostratigraphic succession is observed in south Sifnos, where the Greenschist subunit, which in terms of protolith is equivalent to the MVS subunit in north Sifnos, is overlain by the Marble subunit. Note that the brittle extensional detachment, which defines the contact between the Main Marble subunit and the underlying Greenschist subunit in south Sifnos, is characterized by limited displacement (Ring et al. 2011) revealing minor disruption of the primary tectonostratigraphic association. Therefore, it seems possible that D_1 ductile deformation was accomplished by shearing parallel to the layering of the original tectonostratigraphic succession.

Another critical question is whether the present WNW–ESE orientation of transport lineation (L_2) is original or it is the result of reorientation due to overprinting of D_2 fabrics by the subsequent D_3 deformation. On the basis of the following critical observations, we consider that the recorded top-to-the-ESE sense of shear reflects the original transport direction during D_2. (a) Kinematic analysis and measurement of L_2 orientation were selectively carried out in domains of low D_3 deformation. (b) The passive rotation of L_2 lineation on long limbs of F_3 folds is minor inasmuch as the D_3 deformation reuses the S_2 foliation. In such cases, the L_2 should retain its original orientation, provided that D_3 strain is low. (c) D_2 and D_3 stretching directions are perpendicular to each other, and hence, D_2 linear minerals (e.g., glaucophane) defining L_2 should be subjected to rolling rather than rotation in orientation during D_3 deformation. Undoubtedly, the shape preferred orientation (L_2) of linear minerals is disrupted by syn-D_3 dynamic recrystallization, but in this case the L_2 is not recognizable. (d) The projection of L_2 on equal-area nets displays limited scattering of data points and is dominated by a strong maximum

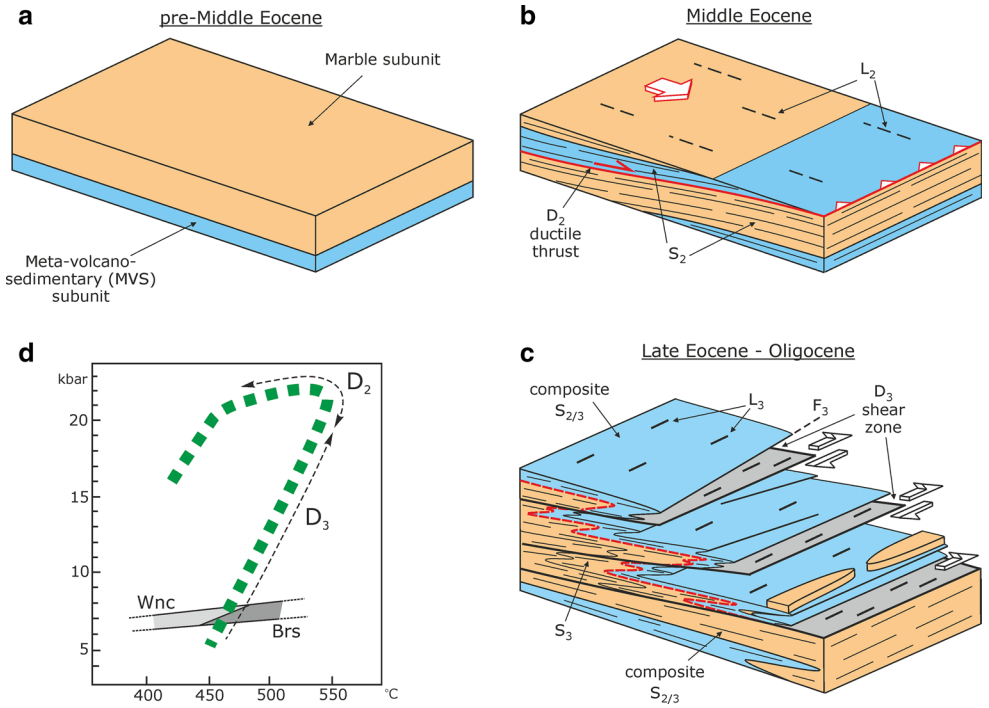

Fig. 11 Block diagrams showing the tectonometamorphic evolution of the CBU in north Sifnos. **a** At the pre-middle Eocene times, the MVS subunit was overlaid by the Marble subunit. **b** Top-to-the-ESE ductile thrusting (D_2) during subduction caused the duplication of the early tectonostratigraphic succession bringing the MVS subunit over the Marble subunit at the middle Eocene times. **c** Development of F_3 folds and restacking of the early nappe pile by NE-directed ductile shear zones during exhumation at Late Eocene–Oligocene times. **d** Generalized pressure (P)–temperature (T) path (dashed line) which summarizes the proposed P–T paths for the CBU in Sifnos (see *inset* in Fig. 1c for details). The potential P–T conditions where the D_2 and D_3 deformation phases occurred are also shown. The *shaded areas* indicate the approximate stability fields of winchite (Wnc) and barroisite (Brs) (after Otsuki and Banno 1990 and references therein)

(Fig. 4b), which is not expected for a strongly reoriented linear fabric. (e) As discussed below, a similar ESE-trending lineation has also been recorded in fresh blueschists cropping out in other Cycladic islands (e.g., Ridley 1982; Xypolias et al. 2012).

Microstructural observations coupled with amphibole chemistry analyses show that the syn-kinematic growth of some large and acicular glaucophane grains that define D_2 fabrics is accompanied by a chemical zoning which is indicative of increasing metamorphic pressures. Thus, it seems that ESE-directed thrusting (D_2) was active during burial and prograde metamorphism. This cannot exclude the possibility that D_2 shearing proceeded to peak metamorphic conditions as well as to the very early stages of the rock exhumation. The latter is reinforced by the fact that epidote is also strongly aligned parallel to S_2 foliation in few samples. However, the absence of glaucophane grains with compositional zoning indicative of decreasing pressures implies that D_2 deformation was followed by the subsequent D_3 deformation phase soon after rocks reached the maximum subduction depth. Therefore, it is reasonable to assume that ESE-directed D_2 thrusting was broadly synchronous with the transition from prograde to retrograde path at middle Eocene (Fig. 11b, d) (ca. 46 Ma; Altherr et al. 1979; Dragovic et al. 2015). This assumption is in accordance with the findings of Lister and Raouzaios (1996), who suggested that the S_2 foliation formed at the high pressures of the eclogite facies in north Sifnos. Also, Neubauer and Genser (2004), in a preliminary work, reported an ESE-trending linear fabric in a massive eclogite exposure in Cape Zilomitis.

The thrust pile developed during D_2 was folded by map-scale recumbent to gently inclined folds, oriented parallel to NE–SW-trending transport lineation (L_3), and restacked by NE-directed large-scale ductile shear zones (Fig. 11c). Data for the compositional zoning of amphiboles defining D_3 fabrics in combination with other deformation/metamorphism relationships described above provide clear evidence that D_3 shearing mainly occurred under blueschist- and transitional blueschist/greenschists conditions after the growth of peak metamorphic assemblage. In a major D_3 shear zone (Fig. 3; Psarobitima shear zone) located at the lower structural levels, it seems that mylonitization locally proceeded to greenschist-facies conditions. These results reveal that decompression and exhumation of rocks from blueschist- to greenschist-facies conditions

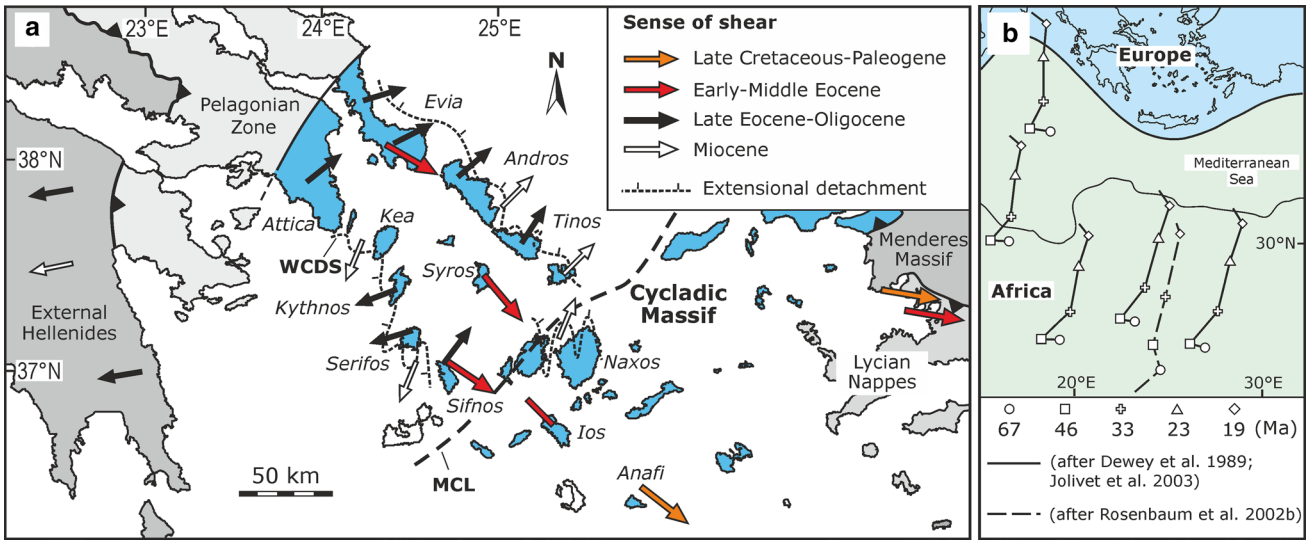

Fig. 12 **a** Simplified geological map of south Aegean region showing the transport direction from Late Cretaceous to Miocene times. Kinematic data after Ridley (1982, 1986), Vandenberg and Lister (1996), Collins and Robertson (1998), Forster and Lister (1999), Rosenbaum et al. (2002a), Rimmelé et al. (2003), Mehl et al. (2007), Xypolias et al. (2010), Grasemann et al. (2012), Xypolias et al. (2012), Weisenbach et al. (2014), Xypolias and Alsop (2014) and this study. WCDS, West Cycladic Detachment System after Grasemann et al. (2012); MCL, Middle Cycladic Lineament after Walcott and White (1998). **b** Simplified map of the eastern Mediterranean region showing the relative motions of Africa and Europe, from late Cretaceous (67 Ma) to early Miocene (19 Ma)

occurred progressively during a single deformation phase (D_3) (Fig. 11c, d). Isotopic dating of phengites from transitional blueschist–greenschist-facies rocks in north Sifnos yielded ages ranging between 41 and 30 Ma (e.g., Wijbrans et al. 1990). Therefore, it is reasonable to assume that this age spectrum possibly corresponds to the period of the main activity of D_3 shear zones in north Sifnos. We speculate that the Psarobitima shear zone, which is dominated by more strongly retrogressed mylonites, should have remained active longer, since equilibration to greenschist-facies conditions occurred at early Miocene. Top-to-the-NE shearing during ductile-stage exhumation of rocks in north and south Sifnos has also been proposed by previous works (Trotet et al. 2001a; Ring et al. 2011). However, we clearly show that the D_3 deformation pattern associated with the top-to-the-NE shearing (Fig. 3) is much more complex than shearing along the lithological boundaries (Fig. 1b; Trotet et al. 2001a) including large-scale folding and restacking of early tectonostratigraphy.

Change in transport direction

An Eocene (W)NW–(E)SE transport direction similar to that described here for the early tectonic evolution of the CBU in Sifnos has been recorded elsewhere in Cyclades area (Fig. 12a). For example, a deformation phase equivalent to D_2 in Sifnos has led to the formation of a SE-trending transport lineation in eclogites/blueschists of Syros (Ridley 1982, 1986; Rosenbaum et al. 2002a). This phase is associated with SE-directed ductile thrusting that mainly occurred during prograde metamorphism and proceeded just after the peak of Eocene (ca. 52 Ma; e.g., Tomaschek et al. 2003) HP metamorphism into close-to-peak retrograde conditions (Ridley 1982, 1986; Keiter et al. 2011; Schumacher et al. 2008). An ESE-directed ductile thrusting that initiated just before and continued at peak metamorphic conditions at Eocene (ca. 45–50 Ma; Maluski et al. 1981), resulting in the stacking of major HP nappes, has been recorded in Evia (Fig. 12a) (Xypolias et al. 2012). A well-developed SE-trending glaucophane lineation developed during Eocene subduction and collision has been recognized in eclogites–blueschists of Ios (Vandenberg and Lister 1996; Forster and Lister 1999). A recent study in Anafi (Weisenbach et al. 2014) reports top-to-the-SE ductile shearing in Late Cretaceous–Paleocene amphibolites of the Uppermost unit. These kinematics reveal that southeastward thrust movements were also dominant at the upper crustal levels of the Cycladic massif during late Cretaceous–Paleogene times. Late Cretaceous to Eocene regional phases of thrusting emplacing the Lycian Nappes over the Menderes Massif (SW Turkey) is also associated with a general top-to-the-ESE transport (Collins and Robertson 1998; Rimmelé et al. 2003). In turn, a consistent (E)NE–(W)SW transport orientation characterizes the Late Eocene–Oligocene tectonic evolution of the Cycladic massif, dominated by the ductile-stage exhumation of the CBU. In the majority of the Cycladic islands, the exhumation-related deformation is accompanied by top-to-the-(E)NE

sense of shear (e.g., Gautier and Brun 1994; Xypolias et al. 2003, 2010; Jolivet et al. 2013), similar to that described for D_3 deformation in Sifnos. (W)SW-directed ductile shearing occurs in west Cyclades (e.g., Grasemann et al. 2012) (Fig. 12a).

From the above, it is conceivable that there is a regional scale change in the tectonic transport direction in Cyclades area from (W)NW–(E)SE at Late Cretaceous–Eocene to (E)NE–(W)SW at Late Eocene–Oligocene times. A change from E–W to N–S compression at the end of Eocene has been proposed by Hall et al. (1984) for the southern Aegean based on kinematic analysis of the Pindos nappe (External Hellenides) in Crete. Such tectonic translation paths that include nearly 90° changes in the direction of nappe movement through time have been described from several orogenic belts and are commonly related to changes in the relative motion between the convergent (micro-) plates and/or indentation tectonics (e.g., Northrup and Burchfiel 1996; Conti et al. 2001; Carosi and Palmeri 2002; Iacopini et al. 2008; Molli and Malavieille 2010). A similar explanation can be given for the observed temporal change in transport direction in Cyclades area based on kinematic models for the relative motion of Africa with respect to Europe during Alpine orogeny. Specifically, kinematic reconstructions have shown that the period between late Cretaceous and middle Eocene (67–46 Ma; Fig. 12b) was characterized by a (W)NW–(E)SE direction of plate motion as well as by a slowdown in the convergence rate, possibly as a result of continental collision in Alps (Dewey et al. 1989; Rosenbaum et al. 2002b; Jolivet et al. 2003). After middle Eocene, the displacement vector changed abruptly following a general NE–SW orientation until at least early Miocene (Fig. 12b).

Exhumation mode

The deformation pattern in north Sifnos for the Late Eocene–Oligocene exhumation of the CBU includes SE-verging map-scale folds oriented at small angle to the NE-trending lineation, as well as (E)NE-directed ductile shear zones that developed parallel to the axial planar foliation (Fig. 11c). Similar deformation pattern with kilometer-scale transport (sub) parallel folds and genetically related shear zones that generated during exhumation of the CBU have been recorded throughout Cycladic massif (Avigad et al. 2001; Ziv et al. 2010; Chatzaras et al. 2011; Xypolias et al. 2012; Xypolias and Alsop 2014). Recently, Xypolias and Alsop (2014) showed that such kilometer-scale folds typically form extensive trains of SE- or NW-directed folds defining large-scale structural domains, which are characterized by consistent fold vergence. Folds of differing vergence (SE- or NW) are generated on the opposite flanks of major antiformal culminations or synformal depressions developed during NE-directed shearing (Xypolias and Alsop 2014; their Fig. 3). By analogy, we assume that NE-verging folds of north Sifnos developed on the flank of such major culmination or depression.

Whether the exhumation-related deformation results from crustal extension or crustal shortening remains, however, to be addressed. Thrusting during exhumation has been proposed by previous work (Lister and Raouzaios 1996) in Sifnos based on the assumption that rocks in north Sifnos subducted at deeper levels than the Greenschist unit in south Sifnos, which occupies lower structural levels of the tectonic pile. It seems, however, that this assumption does not hold since all rocks on Sifnos have been affected by eclogite-facies metamorphism. Therefore, other criteria should be used in order to discriminate the exhumation mode. Our structural mapping in north Sifnos reveals that NE-directed D_3 shear zones cut up-section in their transport direction and repeat the early thrust sequence causing thickening of the tectonic pile. Such a situation is to be expected in contractional belts (e.g., Butler and Freeman 1996), and hence, it seems that D_3 shear zones accommodate net orogenic contraction having operated as ductile thrust zones. Moreover, as pointed by Schmädicke and Will (2003), the recorded P–T paths showing cooling during decompression cannot be explained by an exhumation mechanism of crustal extension but, in turn, require crustal underthrusting beneath the rising HP rocks. Additionally, (a) the absence of downward increase in metamorphic pressure in the CBU (Bröcker et al. 2004), and (b) the absence of Eocene–Oligocene extensional sedimentary basins (e.g., Kokkalas et al. 2006), which are the most reliable criteria of extension-driven exhumation (Platt 1993), point against extensional detachment faulting. Therefore, we suggest that Late Eocene–Oligocene exhumation of the CBU in Sifnos from Eclogite–Blueschist to greenschist-facies conditions was governed by crustal shortening rather than extension as proposed by others (e.g., Trotet et al. 2001a; Jolivet and Brun 2010). Extension seems that contributed to the final exhumation of the CBU in Miocene times, synchronous to the development of the West Cycladic Detachment System (Fig. 12a). Consequently, the most plausible exhumation mechanism is the ductile extrusion of HP rocks between a lower subduction-related thrust fault and an upper crustal-scale normal-sense fault operating in a tectonic setting of net compression, as has been suggested from previous studies in Cyclades (Xypolias et al. 2003, 2010, 2012; Ring et al. 2007).

Conclusions

The integration of geological/structural mapping, microstructural observations and amphibole chemistry analyses

within the CBU in north Sifnos area leads to the following conclusions:

1. Early deformation structures/fabrics, which are recognized in well-preserved eclogites and blueschists, are associated with ESE-directed ductile thrusting that caused duplication of the early tectonostratigraphic succession bringing the MVS over the Marble subunit. Top-to-the-ESE sense of shear occurred under HP conditions and was broadly synchronous with the transition from the prograde to retrograde path at middle Eocene. This middle Eocene transport direction is consistent with kinematics previously recorded in eclogites/blueschists of other Cycladic islands (e.g., Syros, Evia).
2. The subsequent phase of ductile deformation is mainly expressed by NE-trending gently inclined folds as well as by major NE-directed ductile shear zones that cut across the axial planes of folds and restack the early thrust pile. The formation of ductile shear zones seems to have taken place under blueschist- and transitional blueschist-/greenschist-facies conditions during the early exhumation of CBU at late Eocene–early Oligocene times. At deeper structural levels of the study area, mylonites show evidence that deformation proceeded at greenschist–facies conditions, implying that NE-directed shearing remained active since late Oligocene–early Miocene, at least to these levels.
3. New and published kinematic data document a regional scale change in tectonic transport direction of the Alpine nappes in south Aegean region from (W)NW–(S)SE at Late Cretaceous–Eocene to (E)NE–(W)SW at Late Eocene–Oligocene times. This change in direction of nappe movements is possibly governed by an analogous change in the relative motion of Africa with respect to Europe during Alpine orogeny.
4. The exhumation of the CBU seems that occurred under a mechanism of ductile extrusion in a tectonic setting of net compression rather than an exhumation mechanism controlled by syn- and post-orogenic crustal-scale extension, as previously proposed for CBU in Sifnos.

Acknowledgments We would like to thank Franz Neubauer and Rodolfo Carosi for their critical reviews which are helpful clarifying and improving this manuscript. Thanks are also due to GEOTAG AEROVIEW Ltd (www.tripinview.com) for providing us the oblique aerial photograph appeared in Fig. 5c. This work was supported by Grant E045 (awarded to P. Xypolias) from the Research Committee of the University of Patras (Programme K. Karatheodori).

References

Altherr R, Schliestedt M, Okrusch M, Seidel E, Kreuzer H, Harre W, Lenz H, Wendt I, Wagner GA (1979) Geochronology of high-pressure rocks on Sifnos (Cyclades, Greece). Contrib Mineral Petrol 70:245–255

Avigad D (1993) Tectonic juxtaposition of blueschists and greenschists in Sifnos Island (Aegean Sea)—implications for the structure of the Cycladic Blueschist belt. J Struct Geol 15:1459–1469

Avigad D, Matthews A, Evans BW, Garfunkel Z (1992) Cooling during the exhumation of a blueschist terrane: Sifnos (Cyclades), Greece. Eur J Mineral 4:619–634

Avigad D, Garfunkel Z, Jolivet L, Azañon JM (1997) Back-arc extension and denudation of Mediterranean eclogites. Tectonics 16:924–941

Avigad D, Ziv A, Garfunkel Z (2001) Ductile and brittle shortening, extensional-parallel folds and maintenance of crustal thickness in the central Aegean (Cyclades, Greece). Tectonics 20:277–287

Bonneau M (1984) Correlation of the Hellenide nappes in the southeast Aegean and their tectonic reconstruction. Geol Soc Spec Publ 17:517–527

Bröcker M, Pidgeon RT (2007) Protolith ages of meta-igneous and metatuffaceous rocks from the Cycladic Blueschist Unit, Greece: results of a reconnaissance U–Pb zircon study. J Geol 115:83–98

Bröcker M, Bieling D, Hacker B, Gans P (2004) High-Si phengite records the time of greenschist facies overprinting: implications for models suggesting mega detachments in the Aegean Sea. J Metamorph Geol 22:427–442

Bröcker M, Baldwin S, Arkudas R (2013) The geological significance of 40Ar/39Ar and Rb–Sr white mica ages from Syros and Sifnos, Greece: a record of continuous (re)crystallization during exhumation? J Metamorph Geol 31:629–646

Brown EH (1977) The crossite content of Ca-amphibole as a guide to pressure of metamorphism. J Petrol 18:53–72

Butler RWH, Freeman S (1996) Can crustal extension be distinguished from thrusting in the internal parts of mountain belts? A case history of the Entrelor shear zone, Western Alps. J Struct Geol 18:909–923

Carman JH, Gilbert MC (1983) Experimental studies on glaucophane stability. Am J Sci 283A:414–437

Carosi R, Palmeri R (2002) Orogen-parallel tectonic transport in the Variscan belt of northeastern Sardinia (Italy): implications for the exhumation of medium-pressure metamorphic rocks. Geol Mag 139(5):497–511

Chatzaras V, Xypolias P, Kokkalas S, Koukouvelas I (2011) Oligocene–miocene thrusting in central Aegean: insights from the Cycladic island of Amorgos. Geol J 46:619–636

Chatzaras V, Dörr W, Finger F, Xypolias P, Zulauf G (2013) U–Pb single zircons ages and geochemistry of metagranitoid rocks in the Cycladic Blueschist (Evia Island): implications for the Triassic tectonic setting of Greece. Tectonophysics 595–596:125–139

Collins AS, Robertson AHF (1998) Processes of late cretaceous to late miocene episodic thrust-sheet translation in the Lycian Taurides, SW Turkey. J Geol Soc Lond 155:759–772

Conti P, Carmignani L, Funedda A (2001) Change of nappe transport direction during the Variscan collisional evolution of central-southern Sardinia (Italy). Tectonophysics 332:255–273

Davis EN (1966) Der geologische Bau der Insel Siphnos. Geol e Geophys Res Athens 10:161–220

Davis BK (1995) Regional-scale foliation reactivation and re-use during formation of a macroscopic fold in the Robertson River Metamorphics, north Queensland, Australia. Tectonophysics 242:293–311

Dewey JF, Helman ML, Turco E, Hutton DHW, Knott SD (1989) Kinematics of the western Mediterranean. In: Coward MP, Dietrich D, Park RG (eds) Alpine tectonics. Geological Society London Special Publication, London, pp 265–283

Dilek Y, Furnes H, Shallo M (2007) Suprasubduction zone ophiolite formation along the periphery of Mesozoic Gondwana. Gondwana Res 11:453–475

Doutsos T, Piper G, Boronkay K, Koukouvelas I (1993) Kinematics of the central Hellenides. Tectonics 12:936–953

Dragovic B, Samanta LM, Baxter EF, Selverstone J (2012) Using garnet to constrain the duration and rate of water-releasing metamorphic reactions during subduction: an example from Sifnos, Greece. Chem Geol 314–317:9–22

Dragovic B, Baxter EF, Caddick MJ (2015) Pulsed dehydration and garnet growth during subduction revealed by zoned garnet geochronology and thermodynamic modeling, Sifnos, Greece. Earth Planet Sci Lett 413:111–122

Dürr S (1986) Das Attisch – Kykladische Kristallin. In: Jacobshagen V (ed) Geologie von Griechenland. Bornträger, Berlin, pp 116–148

Evans BW (1986) Reactions among sodic, calcic, and ferromagnesian amphiboles, sodic pyroxene, and deerite in high-pressure metamorphosed ironstone, Siphnos, Greece. Am Mineral 71:1118–1125

Evans BW (1990) Phase relations of epidote–blueschists. Lithos 25:3–23

Forster MA, Lister GS (1999) Detachment faults in the Aegean core complex of Ios, Cyclades, Greece. Geol Soc Spec Publ 154:305–323

Forster MA, Lister GS (2005) Several distinct tectono-metamorphic slices in the Cycladic Eclogite–Blueschist belt, Greece. Contrib Mineral Petrol 150:523–545

Forster M, Lister G (2009) Core-complex-related extension of the Aegean lithosphere initiated at the Eocene–Oligocene transition. J Geophys Res: Solid Earth. doi:10.1029/2007JB005382

Franz L, Okrusch M, Bröcker M (1993) Polymetamorphic evolution of pre-Alpidic basement rocks on the island of Sikinos (Cyclades, Greece). N Jb Miner Mh 4:145–162

Ganor J, Matthews A, Paldor N (1989) Constraints of effective diffusivity during oxygen isotope exchange at a marble–schist contact, Sifnos (Cyclades), Greece. Earth Planet Sci Lett 94:208–216

Gautier P, Brun JP (1994) Crustal-scale geometry and kinematics of late-orogenic extension in the central Aegean (Cyclades and Evvia Island). Tectonophysics 238:399–424

Godin L, Grujic D, Law RD, Searle MP (2006) Channel flow, ductile extrusion and exhumation in continental collision zones: an introduction. In: Law RD, Searle MP, Godin L (eds) Channel flow, ductile extrusion and exhumation in continental collision zones, vol 268. Geological Society London Special Publications, London, pp 1–23

Grasemann B, Schneider DA, Stöckli DF, Iglseder C (2012) Miocene divergent crustal extension in the Aegean: evidence from the western Cyclades (Greece). Lithosphere 4:23–39

Groppo C, Forster M, Lister G, Compagnoni R (2009) Glaucophane schists and associated rocks from Sifnos (Cyclades, Greece): new constrains on the P–T evolution from oxidized systems. Lithos 109:254–273

Hall R, Audley-Charles MG, Carter DJ (1984) The significance of Crete for the evolution of the eastern Mediterranean. Geol Soc Spec Publ 17:499–516

Hodges KV, Parrish R, Housh T, Lux D, Burchfiel BC, Royden L, Chen Z (1992) Simultaneous Miocene extension and shortening in the Himalayan orogen. Science 258:1466–1470

Iacopini D, Carosi R, Montomoli C, Passchier CW (2008) Strain analysis and vorticity of flow in the Northern Sardinian Variscan belt: recognition of a partitioned oblique deformation event. Tectonophysics 446:77–96

Jacobshagen V (1986) Geologie von Griechenland. Borntraeger, Stuttgart

Jolivet L, Brun ZJP (2010) Cenozoic geodynamic evolution of the Aegean. Int J Earth Sci 99:109–138

Jolivet L, Faccenna C, Goffé B, Burov E, Agard P (2003) Subduction tectonics and exhumation of high-pressure metamorphic rocks in the Mediterranean orogens. Am J Sci 303:353–409

Jolivet L, Faccenna C, Huet B, Labrousse L, Le Pourhiet L, Lacombe O, Lecomte E, Burov E, Denèle Y, Brun JP, Philippon M, Paul A, Salaün G, Karabulut H, Piromallo C, Monié P, Gueydan F, Okay AI, Oberhänsli R, Pourteau A, Augier R, Gadenne L, Driussi O (2013) Aegean tectonics: strain localisation, slab tearing and trench retreat. Tectonophysics 597–598:1–33

Katzir Y, Avigad D, Matthews A, Garfunkel Z, Evans BW (2000) Origin, HP/LT metamorphism and cooling of ophiolitic mélanges in southern Evia (NW Cyclades), Greece. J Metamorph Geol 18:699–718

Keiter M, Piepjohn K, Ballhaus C, Lagos M, Bode M (2004) Structural development of high-pressure metamorphism rocks on Syros island (Cyclades, Greece). J Struct Geol 26:1433–1445

Keiter M, Ballhaus C, Tomaschek F (2011) A new geological map of the Island of Syros (Aegean Sea, Greece): implications for lithostratigraphy and structural history of the Cycladic Blueschist Unit. Geol Soc Am Spec Pap 481:1–43

Kilias A, Frisch W, Avgerinas A, Dunkl I, Falalakis G, Gawlick HJ (2010) Alpine architecture and kinematics of deformation of the northern Pelagonian nappe pile in the Hellenides. Austrian J Earth Sci 103:4–25

Kokkalas S, Xypolias P, Koukouvelas I, Doutsos T (2006) Post-collisional contractional and extensional deformation in the Aegean region. In: Dilek Y, Pavlides S (eds) Post-collisional tectonics and magmatism in the eastern Mediterranean Region, vol 409. Geological Society America Special Publications, New York, pp 97–123

Kruckenberg SC, Vanderhaeghe O, Ferré EC, Teyssier C, Whitney DL (2011) Flow of partially molten crust and the internal dynamics of a migmatite dome, Naxos, Greece. Tectonics 30:TC3001. doi:10.1029/2010TC002751

Laird J, Albee AL (1981) Pressure, temperature, and time indicators in mafic schist; their application to reconstructing the polymetamorphic history of Vermont. Am J Sci 281:127–175

Leake BE, Woolley AR, Arps CES et al (1997) Nomenclature of amphiboles: report of the Subcommittee on Amphiboles of the International Mineralogical Association, commission on new minerals and mineral names. Can Mineral 35:219–246

Lister G, Raouzaios A (1996) The tectonic significance of a porphyroblastic blueschist facies overprint during Alpine orogenesis: Sifnos, Aegean Sea, Greece. J Struct Geol 18:1417–1435

Maluski H, Vergely P, Bavay D, Bavay P, Katsikatsos G (1981) 39Ar/40Ar dating of glaucophanes and phengites in southern Euboa (Greece): geodynamic implications. Bull Soc Géol Fr 18(23):469–476

Maruyama S, Liou JG, Terabayashi M (1996) Blueschist and eclogites of the world and their exhumation. Int Geol Rev 38:485–594

Matthews A, Schliestedt M (1984) Evolution of the blueschist and greenschist facies rocks of Sifnos, Cyclades, Greece. Contrib Mineral Petrol 88:150–163

Mehl C, Jolivet L, Lacombe O, Labrousse L, Rimmele G (2007) Structural evolution of Andros (Cyclades, Greece): a key to the behavior of a (flat) detachment within an extending continental crust. The geodynamics of the Aegean and Anatolia, vol 291. Geological Society Special Publication, London, pp 41–73

Mocek B (2001) Geochemical evidence for arc-type volcanism in the Aegean Sea: the blueschist unit of Siphnos, Cyclades (Greece). Lithos 57:263–289

Molli G, Malavieille J (2010) Orogenic processes and the Corsica/Apennines geodynamic evolution: insights from Taiwan. Int J Earth Sci (Geol Rundsch). doi:10.1007/s00531-010-0598-y

Montomoli C, Iaccarino S, Carosi R, Langone A, Visona D (2013) Tectonometamorphic discontinuities within the Greater Himalayan Sequence in Western Nepal (Central Himalaya): insights on the exhumation of crystalline rocks. Tectonophysics 608:1349–1370

Mountrakis D (1986) The Pelagonian Zone in Greece: a polyphase-deformed fragment of the Cimmerian continent and its role in the geotectonic evolution of the eastern Mediterranean. J Geol 94:335–347

Neubauer F, Genser J (2004) Microfabric evolution of high-pressure rocks during subduction and exhumation: Sifnos, Aegean Sea. In Proceedings of the 5th international symposium on eastern Mediterranean geology vol 1, international symposium on East Mediterranean Geology Org Comm, Thessaloniki, Greece, pp 143–146

Northrup CJ, Burchfiel BC (1996) Orogen parallel transport and vertical partitioning of strain during oblique collision, Efjorden, north Norway. J Struct Geol 18:1231–1244

Okrusch M, Bröcker M (1990) Eclogites associated with high grade blueschists in the Cyclades archipelago, Greece: a review. Eur J Mineral 2:451–478

Otsuki M, Banno S (1990) Prograde and retrograde metamorphism of hematite-bearing basic schists in the Sanbagawa belt in central Shikoku. J Metamorph Geol 8:425–439

Papanikolaou D (2009) Timing of tectonic emplacement of the ophiolites and terrane paleogeography in the Hellenides. Lithos 108:262–280

Papanikolaou D (2013) Tectonostratigraphic models of the Alpine terranes and subduction history of the Hellenides. Tectonophysics 595–596:1–24

Passchier CW, Trouw RAJ (2005) Microtectonics. Springer, Berlin

Platt JP (1993) Exhumation of high-pressure rocks: a review of concepts and processes. Terra Nova 5:119–133

Reinecke T, Altherr R, Hartung B, Hatzipanagiotou K, Kreuzer H, Harre W, Klein H, Keller J, Geenen E, Böger H (1982) Remnants of a Late Cretaceous high temperature belt on the island of Anafi (Cyclades, Greece). N Jb Miner Abh 145:157–182

Ridley J (1982) Arcuate lineation trends in a deep level, ductile thrust belt, Syros, Greece. Tectonophysics 88:347–360

Ridley J (1986) Parallel stretching lineations and fold axes oblique to a shear displacement direction—a model and observations. J Struct Geol 8:647–653

Rimmelé G, Oberhänsli R, Goffé B, Jolivet L, Candan O, Çetinkaplan M (2003) First evidence of high-pressure metamorphism in the "Cover Series" of the southern Menderes Massif. Tectonic and metamorphic implications for the evolution of SW Turkey. Lithos 71:19–46

Ring U, Glodny J, Will T, Thomson SN (2007) An Oligocene extrusion wedge of blueschist-facies nappes on Evia, Aegean Sea, Greece: implications for the early exhumation of high-pressure rocks. J Geol Soc Lond 164:637–652

Ring U, Glodny J, Will T, Thomson S (2010) The hellenic subduction system: high-pressure metamorphism, exhumation, normal faulting, and large-scale extension. Annu Rev Earth Planet Sci 38:45–76

Ring U, Glodny J, Will TM, Thomson S (2011) Normal faulting on Sifnos and the South Cycladic Detachment System, Aegean Sea, Greece. J Geol Soc 168:751–768

Robertson AHF (2002) Overview of the genesis and emplacement of Mesozoic ophiolites in the eastern Mediterranean Tethyan region. Lithos 65:1–67

Robertson AHF, Dixon JE (1984) Introduction: Aspects of the geological evolution of the eastern Mediterranean. In: Robertson AHF, Dixon JE (eds) The geological evolution of the eastern Mediterranean, vol 17. Geological Society Special Publication, London, pp 1–74

Rosenbaum G, Avigad D, Sánchez-Gómez M (2002a) Coaxial flattening at deep levels of orogenic belts: evidence from blueschists and eclogites on Syros and Sifnos (Cyclades, Greece). J Struct Geol 24:1451–1462

Rosenbaum G, Lister GS, Duboz C (2002b) Relative motions of Africa, Iberia and Europe during Alpine orogeny. Tectonophysics 359:117–129

Schliestedt M (1990) Occurrences and stability conditions of low-temperature eclogites. In: Carswell DA (ed) Eclogite Facies Rocks. Chapman & Hall, New York, pp 160–179

Schliestedt M, Matthews A (1987) Transformation of blueschist to greenschist facies rocks as a consequence of fluid infiltration, Sifnos (Cyclades), Greece. Contrib Mineral Petrol 97:237–250

Schmädicke E, Will TM (2003) Pressure–temperature evolution of blueschist facies rock from Sifnos, Greece, and implications for the exhumation of high-pressure rocks in the central Aegean. J Metamorph Geol 21:799–811

Schumacher JC, Brady JB, Cheney JT, Tonnsen RR (2008) Glaucophane-bearing marbles on Syros, Greece. J Petrol 49:1667–1686

Shaked Y, Avigad D, Garfunkel Z (2000) Alpine high-pressure metamorphism at the Almyropotamos window (southern Evia, Greece). Geol Mag 137:367–380

Tomaschek F, Kennedy A, Villa I, Lagos M, Ballhaus C (2003) Zircons from Syros, Cyclades, Greece—recrystallization and mobilization of zircon during high-pressure metamorphism. J Petrol 44:1977–2002

Trotet F, Jolivet L, Vidal O (2001a) Tectonometamorphic evolution of Syros and Sifnos Islands (Cyclades, Greece). Tectonophysics 338:179–206

Trotet F, Vidal O, Jolivet L (2001b) Exhumation of Syros and Sifnos metamorphic rocks (Cyclades, Greece). New constraints on the P–T paths. Eur J Mineral 13:901–920

van Hinsbergen DJJ, Schmid SM (2012) Map view restoration of Aegean–West Anatolian accretion and extension since the Eocene. Tectonics 31:TC5005. doi:10.1029/2012TC003132

Vandenberg LC, Lister GS (1996) Structural analysis of basement tectonites from the Aegean metamorphic core complex of Ios, Cyclades, Greece. J Struct Geol 18:1437–1454

Walcott CR, White SH (1998) Constraints on the kinematics of post-orogenic extension imposed by stretching lineations in the Aegean region. Tectonophysics 298:155–175

Weisenbach B, Martha SO, Dörr W, Petschick R, Xypolias P, Zulauf G (2014) Structural evolution and kinematics of Pelagonian-type crystalline rocks of central Crete and Anafi island. Schriftenreihe Dtsch Ges Geowiss 85:592

Wijbrans JR, York D, Schliestedt M (1990) Single grain argon laser probe dating of phengites from the blueschist to greenschist transition on Sifnos (Cyclades, Greece). Contrib Mineral Petrol 104:582–593

Xypolias P, Alsop GI (2014) Regional flow perturbation folding within an exhumation channel: a case study from the Cycladic Blueschists. J Struct Geol 62:141–155

Xypolias P, Doutsos T (2000) Kinematics of rock flow in a crustal-scale shear zone: implication for the orogenic evolution of the southwestern Hellenides. Geol Mag 137:81–96

Xypolias P, Kokkalas S, Skourlis K (2003) Upward extrusion and subsequent transpression as a possible mechanism for the exhumation of HP/LT rocks in Evia Island (Aegean Sea, Greece). J Geodyn 35:303–332

Xypolias P, Spanos D, Chatzaras V, Kokkalas S, Koukouvelas I (2010) Vorticity of flow in ductile thrust zones: examples from the Attico-Cycladic Massif (Internal Hellenides, Greece). In: Law RD et al (eds) Continental tectonics and mountain building: the legacy of Peach and Horne, vol 335. Geological Society Special Publication, London, pp 687–714

Xypolias P, Iliopoulos I, Chatzaras V, Kokkalas S (2012) Subduction- and exhumation-related structures in the Cycladic Blueschist: insights from south Evia Island (Aegean region, Greece). Tectonics 31:01. doi:10.1029/2011TC002946

Ziv A, Katzir Y, Avigad D, Garfunkel Z (2010) Strain development and kinematic significance of the Alpine folding on Andros (western Cyclades, Greece). Tectonophysics 488:248–255

Zulauf G, Klein T, Kowalczyk G, Krahl J, Romano S (2008) The Mirsini syncline of eastern Crete, Greece: a key area for understanding pre-Alpine and Alpine orogeny in the eastern Mediterranean. Z Dtsch Ges Geowiss 159:399–414